Influence of Storm–Storm and Storm–Environment Interactions on Tropical Cyclone Formation and Evolution

JAMES P. FOWLER AND THOMAS J. GALARNEAU JR.

Department of Hydrology and Atmospheric Sciences, The University of Arizona, Tucson, Arizona

(Manuscript received 12 May 2017, in final form 30 September 2017)

ABSTRACT

The aim of this study is to examine the development of four tropical cyclones (TCs) in the North Atlantic basin in late August and early September 2010. This period is of interest because four consecutive easterly waves emerged from West Africa and resulted in a multiple TC event (MTCE) over the North Atlantic. The first two TCs—Danielle and Earl—quickly developed into TCs east of 40°W and eventually intensified into major hurricanes. Conversely, the last two TCs—Fiona and Gaston—developed more slowly reaching only weak tropical storm intensity at their peak. The close proximity and differing evolution of these four TCs provides a unique opportunity to examine how these TCs interacted with each other and their surrounding environment, which influenced their development as they moved westward across the North Atlantic. The results showed that concurrent extratropical cyclogenesis events over the western and eastern North Atlantic and the recurvature of TC Danielle produced increased meridional flow over the midlatitude North Atlantic. This increased meridional flow resulted in subsynoptic-scale regions of increased vertical wind shear in the subtropics, which delayed Earl's development and led to Fiona's demise. Additionally, increased meridional flow in midlatitudes contributed to anomalous drying of the subtropics. This dry air was entrained into Gaston's circulation leading to reduced convection and weakening. These TC–TC and TC–environment interactions highlight the difficult challenge of forecasting TC genesis and position posed by MTCEs in a rapidly evolving synoptic-scale flow.

1. Introduction

In late August and early September 2010 four African easterly waves (AEWs) developed into tropical cyclones (TCs) in the main development region of the North Atlantic basin. These TCs all developed east of 45°W within the 10-day period of 21 August through 1 September (Fig. 1). The first two TCs, Danielle and Earl, both reached category 4 on the Saffir–Simpson hurricane wind scale (Simpson and Saffir 1974). The last two TCs, Fiona and Gaston, remained weak tropical storms as they moved westward across the tropical and subtropical Atlantic. The close proximity in time and space of these four TCs, as shown by the time–longitude diagram of 700-hPa meridional wind[1] (averaged in the 10°–20°N latitude band) in Fig. 1, supports the assertion that this period is a multiple TC event (MTCE) as described by Krouse and Sobel (2010, and references within), Schenkel (2016), and Schenkel (2017). The four TCs moved over the Atlantic within a rapidly evolving synoptic-scale flow pattern. TC Danielle developed when the midlatitude and subtropical flow was primarily zonal, while TCs Earl, Fiona, and Gaston interacted with several upper-level cyclonic circulations and abundant dry air in the subtropics as the flow became more meridional. The aim of this study is to examine the multiscale processes associated with synoptic-scale flow amplification over the North Atlantic, and how each of these TCs interacted with the environment. We also aim to show that the TCs themselves contributed to amplification of the synoptic-scale flow pattern that impacted the development of subsequent TCs.

The favorable conditions for TC genesis typically include warm sea surface temperatures ≥26.5°C, moist conditions at midlevels, strong divergence at upper levels, deep-layer vertical wind shear ≤12.5 m s^{-1}, and a preexisting low-level cyclonic disturbance (Gray 1968).

[1] The time–longitude diagram in Fig. 1 is derived from the Climate Forecast System Reanalysis (Saha et al. 2010). A description of datasets used is provided in section 2.

Corresponding author: Thomas J. Galarneau Jr., tgalarneau@email.arizona.edu

DOI: 10.1175/MWR-D-17-0131.1

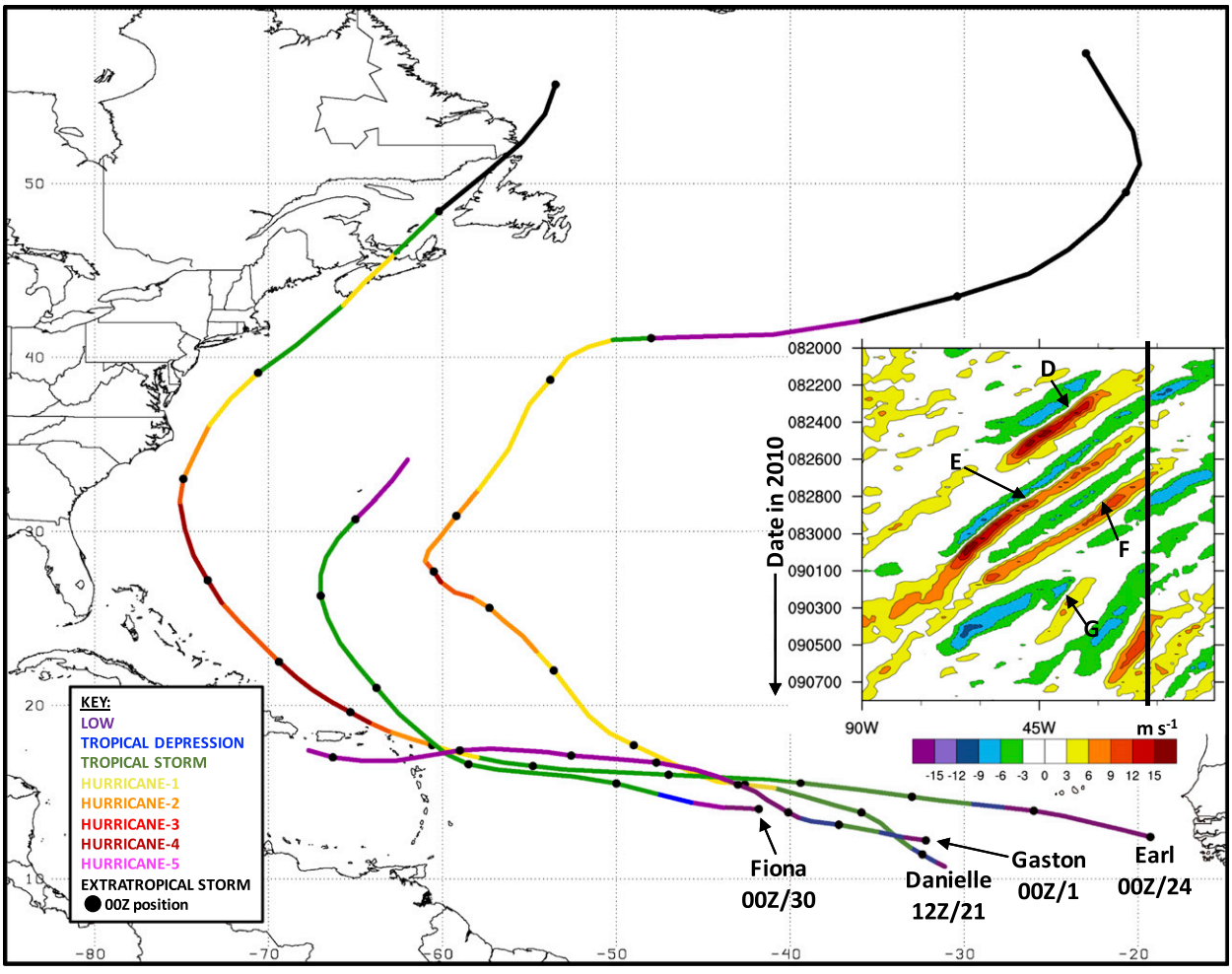

FIG. 1. HURDAT positions and storm classification for TCs Danielle, Earl, Fiona, and Gaston. The 0000 UTC positions are marked by a black-filled circle, and classifications are colored according to the key inset in the bottom left. (right inset) Time–longitude diagram of 700-hPa meridional wind (shaded in m s^{-1}) averaged in the 10°–20°N latitude band. Cyclonic horizontal shear couplets corresponding to Danielle (D), Earl (E), Fiona (F), and Gaston (G) are indicated. The west coast of Africa is marked by a solid black line.

In the North Atlantic basin, the preexisting low-level disturbance can be associated with, for instance, AEWs (Kiladis et al. 2006), extratropical cyclones (Davis and Bosart 2003), and continental mesoscale convective systems (Bosart and Sanders 1981). Researchers and forecasters have long sought to understand what distinguishes which preexisting low-level disturbances will develop into TCs (Tory and Frank 2010). A recurring finding is that initial intensity is a strong predictor of eventual TC genesis (McBride and Zehr 1981). The recently developed Marsupial Paradigm (Dunkerton et al. 2009) embraces the idea that the stronger systems on the disturbance scale, which we will consider resolvable by global reanalysis datasets, will tend to develop by creating strong recirculation regions that offer more dynamical insulation of enhanced water vapor from surrounding dry air and vertical wind shear. This dynamically insulated region is referred to as the ''marsupial pouch'' (or ''pouch'') and represents the meso-α- to synoptic-scale region of the disturbance within which the meso-β-scale TC develops.

The actual TC that forms typically has a radius of maximum winds closer to 100 km or less, considerably smaller than the pouch scale.[2] This smaller scale is not well represented in gridded reanalysis datasets, or earlier rawinsonde-based studies of genesis (e.g., Reed et al. 1977). Thus, studies of genesis from reanalysis data intrinsically examine ''pouch scale'' structures rather than ''TC scale'' structures. The distinction is often fuzzy

[2] In alignment with Orlanski (1975), the pouch scale is equivalent to meso-α to synoptic scale and TC scale is equivalent to meso-β scale.

because both pouches and TCs come in a wide range of scales. Case studies have recently noted that the innermost 100–200 km of the pouch undergoes the most obvious thermodynamic and circulation changes prior to genesis (e.g., Smith and Montgomery 2012; Davis and Ahijevych 2012, 2013; Komaromi 2013). We assume that this ''inner pouch'' (Wang 2012) represents processes on the TC scale. Although composites that sample the inner pouch exist (Zawislak and Zipser 2014), data are currently not sufficient to examine thermodynamic and kinematic structures for a number of cases sufficient to distinguish differing environmental influences on TC-scale processes. Predictability studies have demonstrated that, for a range of commonly observed environmental conditions, one can obtain radically different outcomes even starting with exactly the same vortex by adding random noise (Tao and Zhang 2014). Clearly, there is a limit to how much we can anticipate genesis by examining environmental characteristics and the pouch-scale vortex properties.

Despite the limits in using reanalysis data to study TC genesis, it is still useful to characterize thermodynamic and kinematic structure on the pouch-scale and the larger-scale surrounding environment. Recent studies of AEW development in the central and eastern Atlantic have indicated that environment moisture in the subtropics just north and west of AEWs modulates whether the AEW will develop into a TC. Brammer and Thorncroft (2015) demonstrated that increased moisture in this region favors TC development. This result is consistent with the idealized modeling studies of TC development in easterly vertical wind shear with dry air located north of the disturbance as is typical of the eastern North Atlantic (Ge et al. 2013). The dry air limits convection in the downshear region, reducing the vigor of the secondary circulation that acts to reduce downshear tilt of the vortex. Genesis is more likely when the air mass in the downshear region is moist, or if the vertical shear is westerly with dry air located north of the disturbance (see also Rappin and Nolan 2012). Interestingly, Hopsch et al. (2010) suggested that AEWs may not develop when the cyclonic circulation is too strong, which enhances the equatorward advection of this dry air in the downshear-right region leading to entrainment into the disturbance's circulation. This result seems at odds with other studies that have shown that intensity of the precursor disturbance is the strongest predictor of eventual TC development (e.g., McBride and Zehr 1981), with the caveat that Hopsch et al. (2010) examined AEWs in strong meridional relative humidity gradients near the African coast. Thus, it appears that the interaction between tropical disturbances and the surrounding environment in the tropical and subtropical Atlantic is quite complex and worthy of continued study.

The environment in which TCs develop in the North Atlantic is modulated by the midlatitude and subtropical synoptic-scale flow (e.g., Bracken and Bosart 2000). Highly amplified synoptic-scale flow patterns in the North Atlantic can occur in conjunction with Rossby wave trains (RWTs) that originate over the western North Pacific (e.g., Orlanski and Sheldon 1995). These RWTs terminate over the western North Atlantic with anticyclonic wave breaking, which drives upper-level troughs into the subtropical North Atlantic (e.g., Thorncroft et al. 1993). A subset of these upper-level troughs are associated with extreme rain events (Massacand et al. 1998; Bosart et al. 2017) and TC genesis (Galarneau et al. 2015). The synoptic-scale flow pattern in the North Atlantic can also become amplified even in the absence of a RWT originating in the Pacific. The amplification is typically driven by extratropical cyclogenesis (e.g., Dickinson et al. 1997) and the extratropical transition of TCs (e.g., Atallah and Bosart 2003) in the western North Atlantic. Advection of potential vorticity by the irrotational wind, linked to latent heating associated with a transitioning TC, can perturb the midlatitude jet by increasing the upper-level PV gradient (Archambault et al. 2013, 2015; Grams and Archambault 2016). The increasing PV gradient and attendant jet intensification drives amplification of the downstream synoptic-scale flow (e.g., Riemer and Jones 2010; Torn and Hakim 2015; Bosart et al. 2017). The amplification can increase the vertical wind shear and impact the available moisture in the surrounding subtropical environment of subsequent tropical disturbances over the central and eastern Atlantic.

The close proximity of TCs Danielle, Earl, Fiona, and Gaston in time and space provides a unique opportunity to study and characterize how these TCs interact with each other and the surrounding rapidly evolving synoptic-scale flow pattern during an MTCE. Additionally, the synoptic-scale flow amplification over the North Atlantic that was initiated by extratropical cyclogenesis over eastern North America and the recurvature of TC Danielle began a period of anomalously low medium-range forecast skill. The day-3 anomaly correlation for control forecasts of 500-hPa geopotential height from the National Oceanic and Atmospheric Administration (NOAA) Global Ensemble Forecast System (GEFS) reforecast dataset (Hamill et al. 2013) remained within 1.0 standard deviation of the 1985–2016 climatology (Fig. 2). The day-5 anomaly correlation, however, was anomalously low for 0000 UTC 28 August–4 September 2010, exceeding −1.0

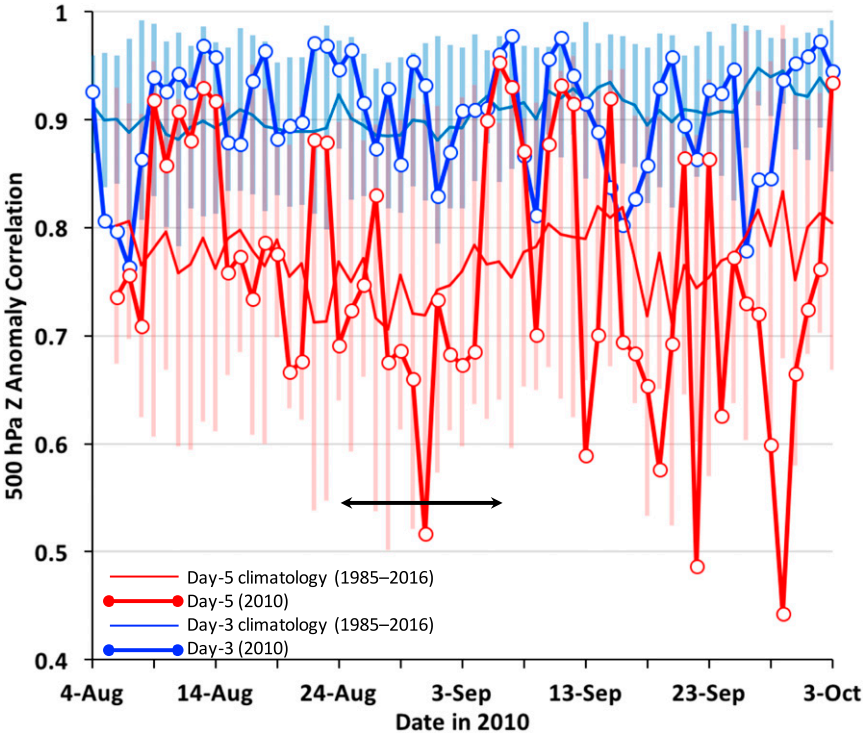

FIG. 2. Time series of the day-3 (blue) and day-5 (red) 500-hPa geopotential height anomaly correlation in the North Atlantic basin (10°–40°N, 80°–10°W) for the control member of the GEFS reforecast dataset for 4 Aug–3 Oct 2010 (thick lines). The 1985–2016 long-term climatology of 500-hPa anomaly correlation values are shown by thin lines, with error bars denoting ±1.0 standard deviation. The black double-sided arrow marks the period of interacting TCs in this study.

standard deviation for the forecast verifying at 0000 UTC 31 August 2010. Bosart et al. (2017) showed a similar reduction in forecast skill for the GEFS reforecasts for a series of extreme weather events over North America and the North Atlantic in October 2007. One of the extreme weather events involved the interaction of TC Noel (2007) with rapidly evolving synoptic-scale flow. An analysis of the GEFS forecast initialized at 0000 UTC 26 August 2010 is presented later in the paper. While a comprehensive analysis of all the forecasts initialized during 28 August–4 September 2010 is beyond the scope of this study, the relatively low forecast skill during this period provides additional motivation for investigating the mutual interactions between TCs and their surrounding environment.

This paper is organized as follows. Section 2 describes the datasets used and diagnostic calculations performed. Section 3 presents a large-scale overview of the synoptic flow pattern, while section 4 presents an analysis of the interaction between TCs and their environment. Section 5 examines the impact of dry air on the evolution of the TCs, and section 6 presents an analysis of the GEFS forecast initialized at 0000 UTC 26 August 2010. Section 7 provides the conclusions.

2. Data and methods

The National Centers for Environmental Prediction (NCEP) Climate Forecast System Reanalysis (CFSR; Saha et al. 2010), available four-times-daily at 0.5° × 0.5° horizontal grid spacing on isobaric levels, was the primary data source for the analyses and diagnostics presented in this study. Tropical cyclone track and intensity information on Fig. 1 was obtained from the NHC "best track" hurricane database (HURDAT; Landsea et al. 2004). The NOAA GEFS reforecasts shown in Fig. 2 were obtained from the NOAA/Earth System Research Laboratory.

The meridional flow index (MFI) was computed similarly to the method described by Archambault et al. (2013), and is defined here as the area-average magnitude of the meridional component of the wind on the dynamic tropopause [DT; defined as the 2.0 potential vorticity unit (PVU) surface where 1.0 PVU = 1.0 × 10^{-6} K kg^{-1} m^2 s^{-1}]. The MFI is computed for the

midlatitude North Atlantic encompassing the region 40°–60°N, 60°–10°W. The Lagrangian perspective is provided through air parcel trajectories that are calculated from the CFSR using the NOAA Air Resources Laboratory HYSPLIT trajectory model (Stein et al. 2015).

The computation of vertical wind shear involves the use of vorticity inversion to remove the TC vortex to determine the environmental wind shear. Following the methods of Davis et al. (2008), a Poisson solver is used to invert the vorticity and divergence as

$$\nabla^2\psi = \begin{pmatrix} \zeta & \text{for} & r \le 4^\circ \\ 0 & \text{for} & r > 4^\circ \end{pmatrix} \tag{1}$$

and

$$\nabla^2\chi = \begin{pmatrix} \delta & \text{for} & r \le 4^\circ \\ 0 & \text{for} & r > 4^\circ \end{pmatrix}, \tag{2}$$

where ψ is the streamfunction, χ is the velocity potential, ζ is the relative vorticity, δ is the divergence, and r is the radius from the TC center. From the solutions to (1) and (2), the nondivergent and irrotational wind vectors representing the TC are defined as

$$\mathbf{V}_{\rm nd}(x,y,p) = \hat{k} \times \nabla\psi \tag{3}$$

and

$$\mathbf{V}_{\rm ir}(x,y,p) = \nabla\chi. \tag{4}$$

By subtracting (3) and (4) from the total wind $\mathbf{V}$[3] as follows:

$$\mathbf{V}_{\rm env}(x,y,p) = \mathbf{V}(x,y,p) - \mathbf{V}_{\rm nd}(x,y,p) - \mathbf{V}_{\rm ir}(x,y,p), \tag{5}$$

we have computed the three-dimensional environment wind $\mathbf{V}_{\rm env}$ in which the effect of the TC circulation is removed for a radius r of 4°. We can now compute the environment vertical wind shear $\mathbf{V}_{\rm shear}$ using $\mathbf{V}_{\rm env}$ defined in (5) as follows:

$$\mathbf{V}_{\rm shear}(x,y) = \mathbf{V}_{\rm env}(x,y,p_2) - \mathbf{V}_{\rm env}(x,y,p_1), \tag{6}$$

where subscript "1" refers to 900 hPa and subscript "2" refers to 200 hPa.

3. Large-scale overview

During 16–24 August 2010, a zonal flow pattern was in place in the 40°–50°N latitude band across the entire North Atlantic (Fig. 3a). The MFI for this period was anomalously low with negative anomalies exceeding −1.0 standard deviation on 22–23 August 2010 (Fig. 4). High-latitude anomalous ridging was in place over the western and central North Atlantic at 250 and 850 hPa, while much of the subtropical Atlantic was very moist with PW anomalies approaching +7 mm (Figs. 3a,b). In fact, the subtropical Atlantic was unusually moist for much of the first three weeks of August, with PW anomalies exceeding +1.0 standard deviation (Fig. 4). During this period of favorable thermodynamics in the subtropics and tropical eastern Atlantic, the AEWs that would become TCs Danielle and Earl emerged from Africa and rapidly underwent genesis.

A robust change in the synoptic-scale flow over the midlatitude and subtropical North Atlantic occurred during 25 August–5 September 2010. The midlatitude 250-hPa flow became more meridional, with a +16-dam anomalous ridge over the western Atlantic and a −12-dam anomalous trough over the eastern Atlantic (Fig. 3c). The anomalous trough over the eastern Atlantic was a deep circulation also apparent at 850 hPa (Fig. 3d). The anomalous northerly and northwesterly flow over the central and eastern subtropical Atlantic is consistent with PW anomalies approaching −5 mm in the region. The increased meridional flow over the Atlantic basin during this period represents a synoptic-scale flow regime transition from zonal flow in midlatitudes and a moist subtropical Atlantic during 16–24 August, to anomalous meridional flow in midlatitudes and an anomalously dry subtropical Atlantic during 25 August–5 September (Fig. 4).[4] The pre-TC Fiona and Gaston disturbances emerged from Africa during the later period marked by unfavorable thermodynamic conditions in the subtropical Atlantic (Figs. 3 and 4).

The Hovmöller diagram of DT meridional wind highlights the transition from a zonal to meridional flow pattern over the midlatitude North Atlantic (Fig. 5). While the synoptic-scale flow over the midlatitude Pacific and North America was characterized by strong meridional flow throughout the entire period, weak meridional flow was present over the North Atlantic east of 60°W on 20–27 August. The synoptic-scale flow began to shift to a more amplified meridional flow pattern over the North Atlantic by 27 August in response to extratropical cyclogenesis near 70°W, which appears to be linked to a RWT originating over the west Pacific, and the development of a deep extratropical cyclone over the eastern North Atlantic. The amplified meridional

[3] The total wind $\mathbf{V}$ is the full wind field without the TC vortex removed.

[4] Correlation of PW and MFI (shown in Fig. 4) was −0.67 for 16 August–5 September 2010.

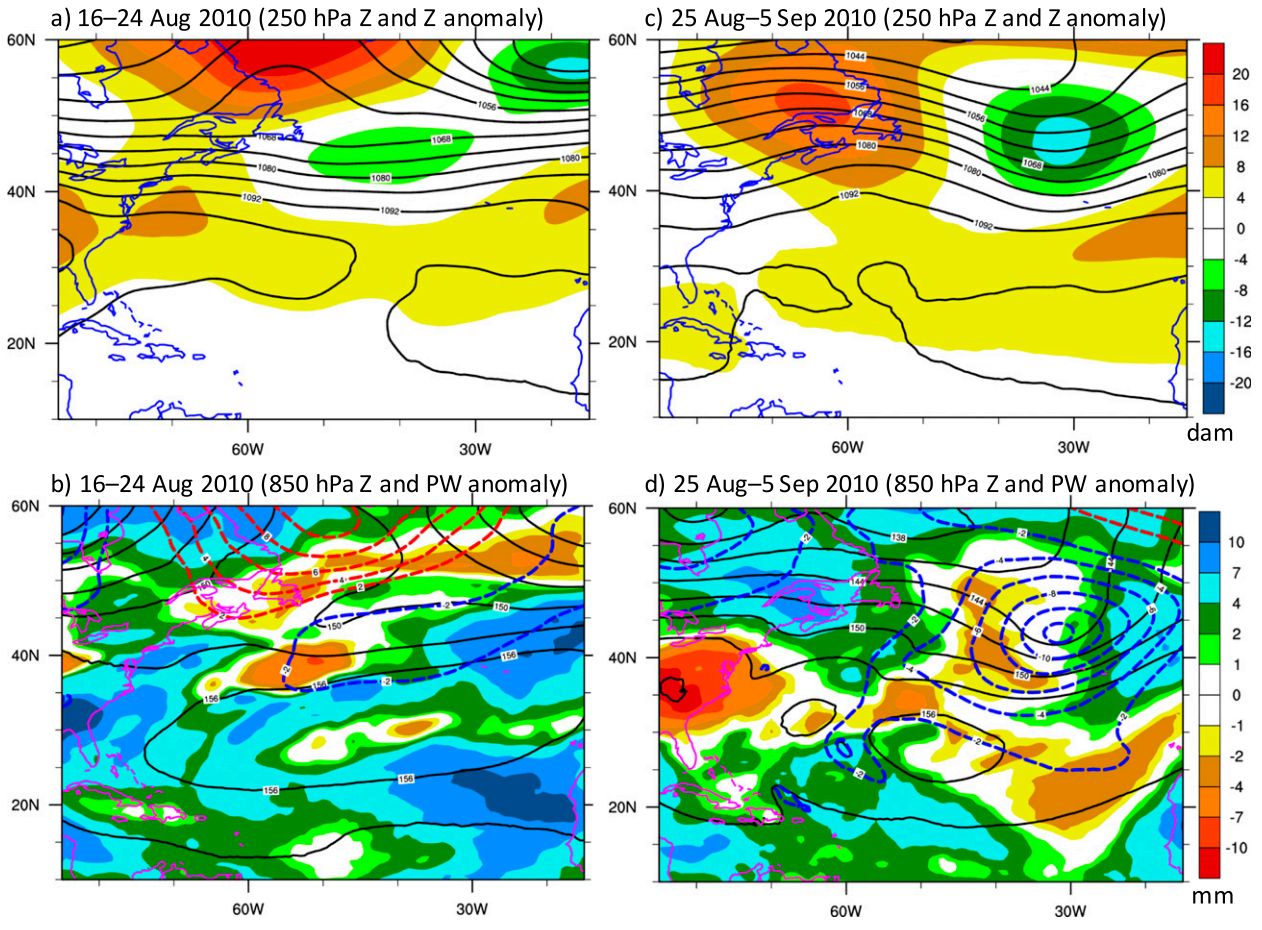

FIG. 3. 250-hPa geopotential height mean (solid contours in dam) and anomaly (shaded in dam) for (a) 16–24 Aug and (c) 25 Aug–5 Sep 2010. 850-hPa geopotential height mean (solid contours in dam) and anomaly (dashed contours in dam, positive in red, negative in blue), and total column PW anomaly (shaded in mm) for (b) 16–24 Aug and (d) 25 Aug–5 Sep 2010. The anomaly is computed from the long-term 1979–2014 mean.

flow over the Atlantic was reinforced as additional RWTs led to the recurvature of TC Danielle after 30 August and TC Earl after 3 September.

In summary, the zonal midlatitude flow pattern over the North Atlantic on 16–24 August abruptly transitioned to a more amplified meridional flow pattern in response to extratropical cyclogenesis events over the east coast of North America and the eastern North Atlantic in conjunction with a RWT that originated over the west Pacific. The recurvature of TCs Danielle and Earl acted to reinforce the amplified meridional flow through early September.

4. TC–environment interactions

The aim of this section is to examine in more detail the complex interactions of the four TCs of interest with the amplified synoptic-scale flow pattern. Figure 6 shows the sea level pressure, 1000–500-hPa thickness, and total column PW for 27 August–3 September 2010. By 0000 UTC 27 August, the midlatitude synoptic-scale flow pattern was characterized by extratropical cyclones located just east of Nova Scotia and over the east-central Atlantic near 40°N, 35°W (Fig. 6a). These cyclones were associated with a RWT that originated over the west Pacific, and marked the transition of a zonal to meridional flow pattern over the North Atlantic (Fig. 5). TC Danielle was at category 2 intensity and located in a ridge environment in the subtropics approximately between the two aforementioned extratropical cyclones. Danielle's warm core structure was well defined as shown by the anticyclonic 900–200-hPa vertical wind shear vectors (TC not removed) and relatively high DT potential temperature (Fig. 7a). Weak upper-level troughs flanked Danielle on its west and east side in the subtropics. The upper-level trough west of Danielle was interacting with Danielle's irrotational outflow, resulting in a sharpening of the PV gradient on its eastern

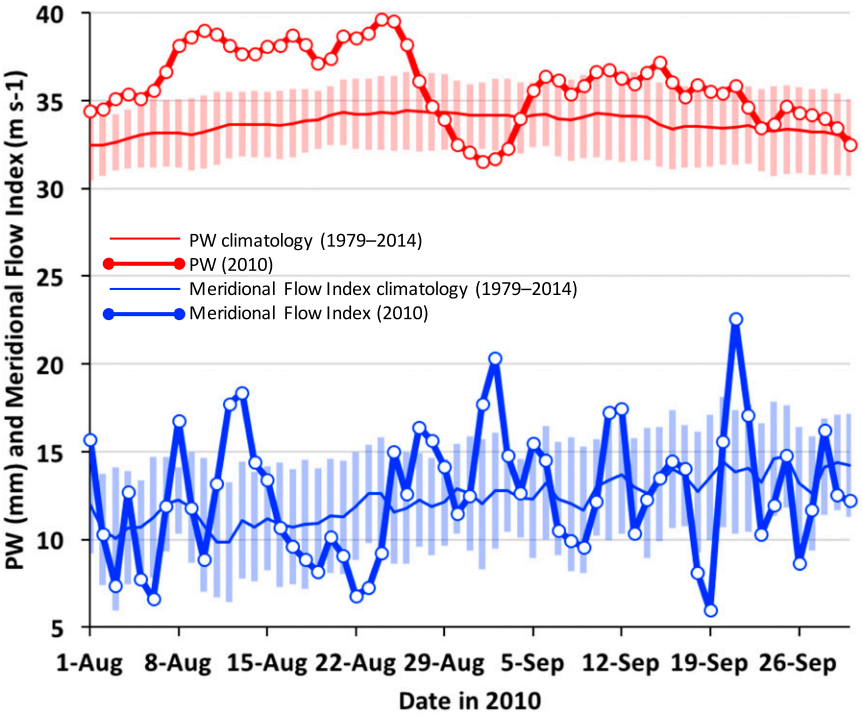

FIG. 4. Time series of the MFI (thick blue line in m s^{-1}; 40°–60°N, 60°–10°W region) and area-mean total column PW (thick red line in mm; 20°–40°N, 60°–10°W region). The 1979–2014 long-term climatology is shown by thin lines, with error bars denoting ±1.0 standard deviation.

flank as a result of negative PV advection by the irrotational wind (Fig. 8a). The upper-level trough east of Danielle reached to just north of TC Earl near 15°N, 40°W. The pre-TC Fiona disturbance had just emerged from over Africa in a fairly moist environment with weak vertical wind shear (Figs. 6a and 7a).

At 0000 UTC 29 August, the upper-level trough that was over eastern North America two days earlier had moved to over the western North Atlantic and began to steer TC Danielle northeastward (Figs. 6b and 7b). The extratropical cyclone over the midlatitude eastern Atlantic deepened to just under 992 hPa, and the northerly and northwesterly flow on the southwest side of this cyclone was driving dry air into the subtropics north of TC Fiona (Fig. 6b). The diabatically driven irrotational outflow from TC Danielle was strongly interacting with the midlatitude trough to the west (Fig. 8b). Additionally, Danielle's outflow was interacting with the upper-level trough to the east as marked by negative PV advection by the irrotational wind. The attendant increased PV gradient contributed to strengthening of the upper-level northerly flow in this region (Fig. 7b).

A Lagrangian perspective on the interaction between Danielle, Earl, and the downstream upper-level trough is shown by 48-h backward air parcel trajectories seeded at 12 000 m above mean sea level (MSL) at grid points over and northeast of TC Earl and along the forward flank of the upper-level trough to the east (Fig. 9a). The air parcels seeded over and northeast of TC Earl originated below 400 hPa within Earl's and Danielle's cyclonic circulation (red trajectory lines) and above 400 hPa within Danielle's outflow anticyclone (green trajectory lines). Air parcel trajectories seeded along the forward flank of the upper-level trough to the east originated above 400 hPa primarily north and east of Danielle (blue trajectory lines). The time series of air parcel potential temperature and pressure for parcels seeded over and northeast of Earl (green) and along the forward flank of the upper-level trough (blue) both cooled and descended through most of their respective paths (Figs. 9b,c). It is noteworthy, however, that air parcels over and northeast of Earl that originated primarily within Danielle's outflow anticyclone were 5 K warmer than the parcels over and along the forward flank of the downstream trough (Fig. 9b). This difference in potential temperature highlights how Danielle's outflow likely helped to maintain and strengthen the near-tropopause thermal gradient (and vertical wind shear) west of the upper-level trough axis and just northeast of Earl. Recall that vertical wind shear associated with the upper-level trough likely delayed Earl's development into an intense TC.

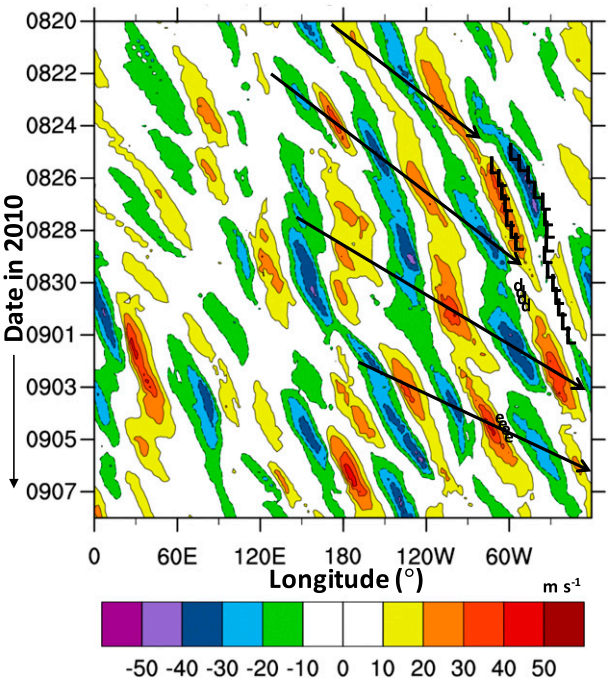

FIG. 5. Time–longitude diagram of DT meridional wind (shaded in m s^{-1}) averaged in the 40°–60°N latitude band. The extratropical cyclones (L), Danielle (d), and Earl (e) are indicated. Selected Rossby wave trains are manually identified by black arrows that approximate the group velocity. The TC positions are labeled for latitude values ≥40°N.

At 0000 UTC 31 August, TC Danielle has moved rapidly northeastward ahead of a strong upper-level trough (Figs. 6c and 7c). Meanwhile, TC Earl moved westward away from the Danielle-influenced subtropical upper-level trough and into a ridge environment (Fig. 7c). As a result, TC Earl began to rapidly intensify and develop a robust warm core structure as shown by the well-defined anticyclonic circulation in the 900–200-hPa vertical wind shear vectors. The burst of convection in Earl's circulation was seen in the upper-level irrotational outflow above Earl, which began to interact with a weak upper-level trough to the north and the aforementioned upper-level trough to the east (Fig. 8c). As Earl rapidly intensified in a weaker steering flow, its forward speed began to slow, allowing TC Fiona to begin to catch up to Earl by 0000 UTC 31 August (Fig. 6c). At the same time, TC Fiona was located in close proximity to the upper-level subtropical trough that Earl interacted with two days earlier (Fig. 7c). Finally, the pre-TC Gaston disturbance emerged from over Africa into a much drier environment in the eastern Atlantic compared to the previous TCs (Fig. 6c).

At 0000 UTC 3 September, TC Earl now an intense category 3 storm was located just east of North Carolina as it began to recurve northeastward in advance of a stout upper-level midlatitude trough over the central United States (Figs. 6d and 7d). This upper-level disturbance was part of another RWT that was triggered over the west Pacific (Fig. 5). A weak TC Fiona was located just southeast of TC Earl at this time, and was in a hostile environment characterized by northeasterly vertical wind shear over 25 m s^{-1} (Fig. 7d). The enhanced vertical wind shear was located on the eastern flank of TC Earl's well-defined warm core structure and upper-level anticyclone and a subtropical trough to the east (Figs. 7d and 8d). A Lagrangian perspective as shown by 48-h air backward air parcel trajectories seeded at 12 000 m MSL over and northeast of TC Fiona at 0000 UTC 3 September demonstrates that air parcels in this region originated from within TC Earl's outflow anticyclone and within the synoptic-scale flow over the central United States (Fig. 9d). The warmer, descending air parcels originating in TC Earl's outflow anticyclone were located just west of cooler, ascending air parcels originating in the midlatitude westerlies (Figs. 9e,f). It is likely that the air parcels from these two source regions acted to maintain and strengthen the upper-level potential temperature gradient on the eastern flank of Earl's outflow anticyclone, thus maintaining the strong vertical wind shear over TC Fiona (leading to Fiona's demise).

Last, TC Gaston moved to near 40°W by 0000 UTC 3 September in an environment that was much drier throughout the subtropics compared to the environment for the earlier TCs (Fig. 6d). The impact of the drier air throughout the subtropics on Gaston's development will be discussed more in the next section.

5. TC moisture evolution

The aim of this section is to examine the intensity and moisture structure of the TCs on the pouch scale. The time series of area-average 600-hPa relative vorticity and 700–500-hPa layer-mean relative humidity in the pouch inner core, and 900–200-hPa vertical wind shear with the TC vortex removed (as described in section 2) is shown in Fig. 10.[5] All four developing TCs reached similar vorticity values near 8×10^{-5} s^{-1} when they reached 40°W. A dramatic departure in intensity of the disturbances was apparent, however, as they continued westward toward 60°W. TCs Danielle and Earl both intensified to strong mature TCs, while Fiona and Gaston

[5] For the time period between the emergence of the pre-TC disturbance from Africa until the first entry in HURDAT, the center of the disturbances was determined by following the CFSR-derived maximum 700-hPa relative vorticity smoothed using a 9-point smoother run 40 times.

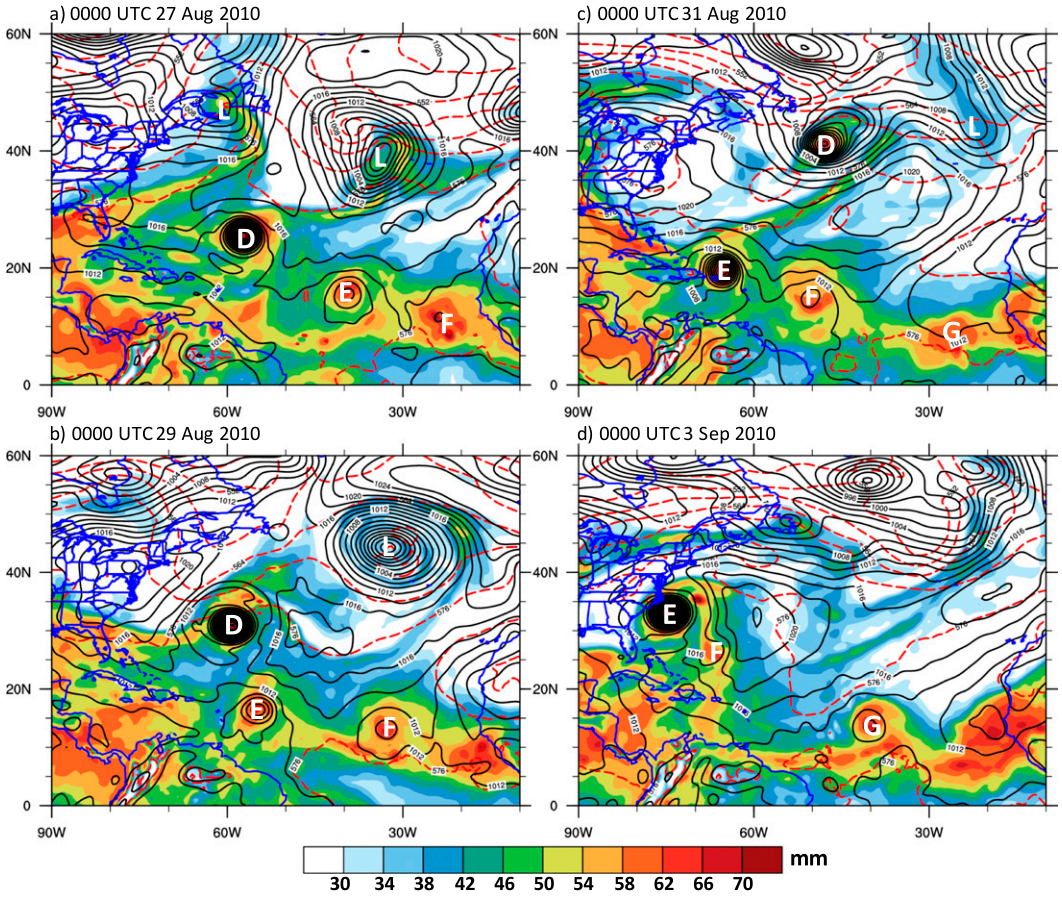

FIG. 6. Total column PW (shaded in mm), sea level pressure (solid contours every 2 hPa), and 1000–500-hPa thickness (dashed red contours every 6 dam) at 0000 UTC (a) 27 Aug, (b) 29 Aug, (c) 31 Aug, and (d) 3 Sep 2010. The extratropical cyclones (L), Danielle (D), Earl (E), Fiona (F), and Gaston (G) are indicated.

gradually weakened. Clearly, the weakening of Fiona and Gaston were related to interactions with TC Earl's outflow for the former and the much drier subtropics for the latter. Note that with exception of a relatively brief period of drying for TC Earl in the presence of northerly and northeasterly vertical wind shear near $10\,m\,s^{-1}$ on 27–29 August, Danielle and Earl remained moist with relative humidity values generally above 80% (Figs. 10a,b). A value of 80% relative humidity has been shown to be sufficient for TC genesis (e.g., Nolan 2007; Davis 2015). While Fiona and Gaston were also moist near 40°W, both systems underwent rapid drying thereafter as they weakened in the presence of northerly vertical wind shear near $15\,m\,s^{-1}$ and easterly shear near $8\,m\,s^{-1}$, respectively (Figs. 10c,d).

A closer inspection of the water vapor surrounding the TCs reveals that the subtropics became drier throughout the period of interest, as discussed earlier. Figure 11 shows time–azimuth plots of area-average 700–500-hPa layer-mean relative humidity in the 2°–10° radial band for all four TCs. The time period shown begins when the pre-TC disturbance emerged from the west coast of Africa and ends with the last entry in HURDAT. The pre-TC Danielle disturbance emerged from Africa in a very moist environment north of the disturbance with 700–500-hPa layer-mean relative humidity values over 80% in a large region (Fig. 11a). The pre-TC Earl and Fiona disturbances emerged from Africa into a slightly drier environment (Figs. 11b,c), while the pre-TC Gaston disturbance moved into an extremely dry environment north of the disturbance with relative humidity values below 35% in a broad region (Fig. 11d).

As these pre-TC disturbances all developed into named TCs as they moved westward, the relative humidity from the northwest (NW) to northeast (NE) azimuths gradually decreased. Within the time period in which there was a departure in TC evolution between 60° and 40°W, TCs Danielle, Earl, and Fiona all had similar distributions of relative humidity from the NW to NE azimuths (Figs. 11a–c). Conversely, TC Gaston had abundant dry air in particular from the north to NE azimuths with a broad region of relative humidity values below 20% (Fig. 11d). The composite vertical structure of area-average relative humidity in the north to NE azimuths

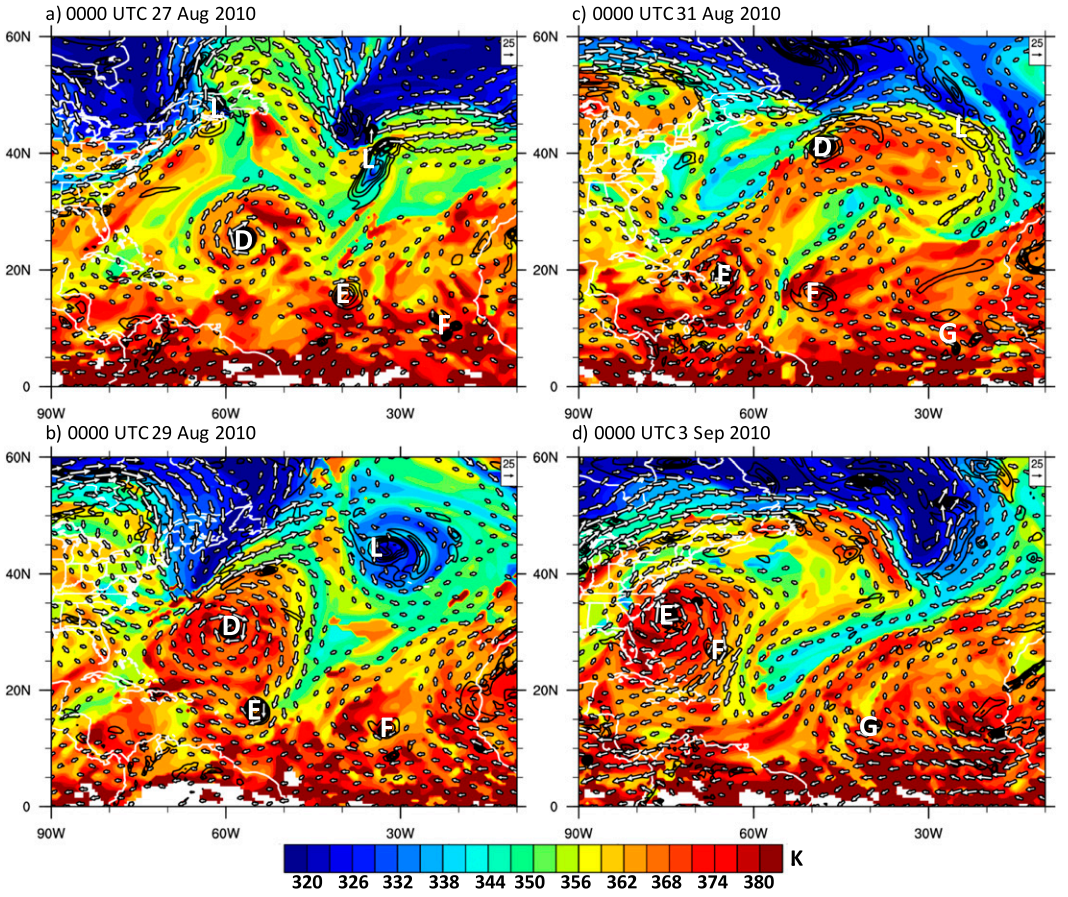

FIG. 7. As in Fig. 6, but showing DT potential temperature (shaded in K), 900–200-hPa vertical wind shear (TC not removed; arrows in $m\,s^{-1}$), and 925–850-hPa layer-mean relative vorticity (solid contours every $4.0 \times 10^{-5}\,s^{-1}$ starting at $4.0 \times 10^{-5}\,s^{-1}$).

time averaged for the 72-h period centered on the time in which the TC was located at 50°W is shown in Fig. 12. Note that all four TCs have similar environment relative humidity values below 800 hPa in this region. Differences arise above 750 hPa, however, with TC Gaston significantly drier than TCs Danielle, Earl, and Fiona above 700 hPa. This result is consistent with dropsonde analyses of Gaston presented by Davis and Ahijevych (2012), and more generally with recent compositing studies of developing and nondeveloping AEWs over the east Atlantic that showed TC genesis is governed by how saturated the environment is poleward of the AEW (Brammer and Thorncroft 2015).

A comparison of the storm-centered composite mean storm-relative streamlines, relative vorticity, and relative humidity vertically averaged in the 700–500-hPa layer for TCs Danielle and Gaston is shown in Fig. 13. The time period used for averaging consists of the 72-h period centered on the time in which the TC was positioned at 50°W. During this period, TC Danielle developed into a mature TC and was characterized by a well-defined moist region of recirculation (i.e., the pouch) in which the smaller-scale TC vortex (not resolvable by the CFSR) was embedded (Fig. 13a). This structure of the pouch is considered favorable for TC development as the inner smaller-scale vortex is insulated from the surrounding dry air in the environment by recirculation in the pouch region (see also Dunkerton et al. 2009). The structure of the pouch in which Gaston was embedded was more unfavorable for TC development (Fig. 13b). The pouch region was considerably smaller compared to Danielle's, and was open to infiltration of very dry air by a northeasterly storm-relative flow on the northeast side of the pouch. Selected storm-relative 84-h backward air parcel trajectories seeded in the 700–500-hPa layer within Gaston's pouch at 1200 UTC 5 September reinforce the results indicated by the storm-relative streamlines (Fig. 13b). In storm-relative coordinates, air parcels within Gaston's pouch originated in the extremely dry air northeast of Gaston and moved into the pouch on the northeast side, thereby representing the pathway in which the anomalously dry air in the subtropics was entrained into Gaston's circulation.

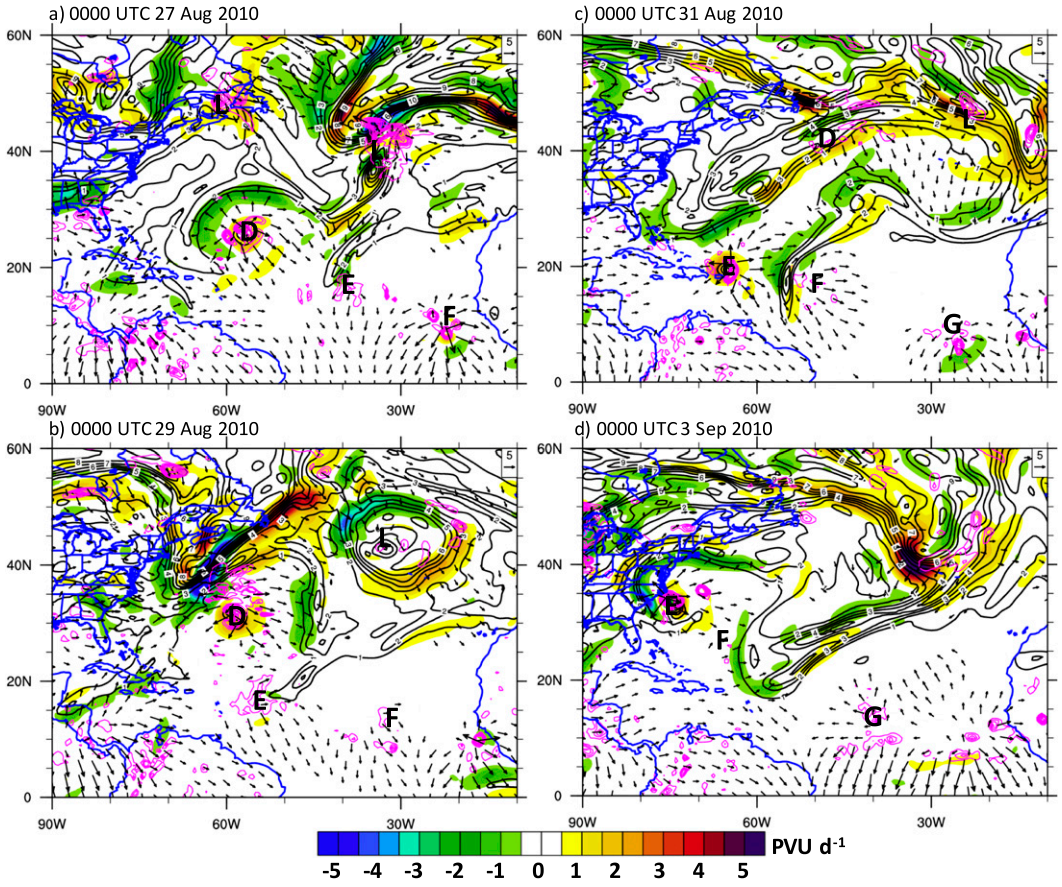

FIG. 8. As in Fig. 6, but showing PV in the 250–150-hPa layer (black contours every 1.0 PVU starting at 1.0 PVU), 250–150-hPa layer-mean irrotational wind (arrows ≥2.5 m s^{-1}), advection of PV by the irrotational wind (shaded in PVU day^{-1}), and 600–400-hPa layer-mean ascent (magenta contours every 0.3 Pa s^{-1} starting at −0.3 Pa s^{-1}).

6. Postscript on GEFS reforecast initialized at 0000 UTC 26 August 2010

a. Overview

The aim of this section is to examine the GEFS reforecast control member initialized at 0000 UTC 26 August 2010, which had the lowest 5-day forecast anomaly correlation coefficient over the North Atlantic in August through mid-September 2010 (Fig. 2). The GEFS track forecasts for Danielle and Earl show that the control forecast was consistent with the envelope of the full 11-member ensemble (Fig. 14a). The GEFS control member track forecast for Danielle moved too far west early in the forecast prior to recurvature at 1200 UTC 28 August (60-h forecast). This westward position error increased with forecast lead, reaching 982 km by 0000 UTC 31 August (120-h forecast) as the observed TC was picked up earlier by the midlatitude westerlies. Conversely, the GEFS control member track forecast for Earl showed an early recurvature error, particularly starting at 1200 UTC 29 August (84-h forecast). The early recurvature error resulted in position errors increasing with forecast lead, reaching 941 km by 0000 UTC 31 August (120-h forecast).

The GEFS 120-h position errors for Danielle and Earl were significantly larger than the track error "baseline" of 400 km calculated from the top-flight operational models for the 2006–08 North Atlantic TC seasons as part of the Hurricane Forecast Improvement Program (HFIP) (Gall et al. 2014). These significant position errors in the 120-h forecast verifying at 0000 UTC 31 August were part of well-defined errors in the midlatitude flow pattern over the North Atlantic region (Fig. 14b). Errors in 500-hPa geopotential height are predominantly associated with TC position errors. Additionally, the ridge–trough couplet located east of Danielle has a westward phase error in the forecast consistent with Danielle's westward position error. While there are no obvious forecast errors in the Rossby wave train originating over the west Pacific (not shown), errors in the TC position and nearby synoptic-scale flow errors are apparent over the midlatitude North Atlantic (Fig. 14b).

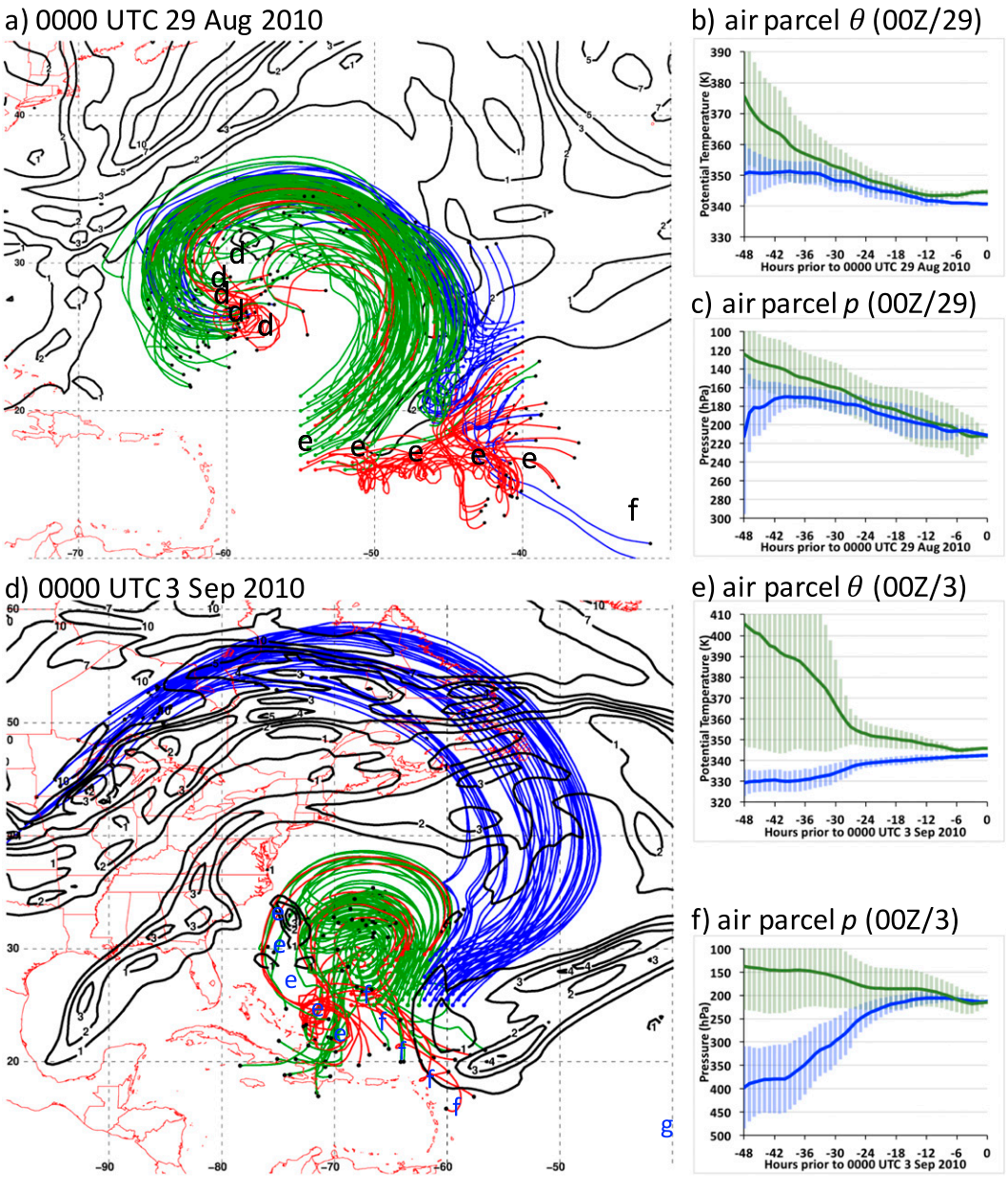

FIG. 9. PV in the 250–150-hPa layer at 0000 UTC (a) 29 Aug and (d) 3 Sep 2010 and positions for 48-h backward air parcel trajectories released from grid points marked by color-filled circles. PV is plotted in black contours at (a) 1.0, 2.0, 3.0, 5.0, 7.0, and 10.0 PVU and (d) every 1.0 PVU starting at 1.0 PVU. The trajectory end points are marked by a black-filled circle. In (a), trajectories with end points located below (above) 400 hPa are in red (green). Trajectories with start points east of the trough axis and end points above 400 hPa are in blue. In (d), trajectories with end points located below (above) 400 hPa are in red (green). All trajectories with end points over North America are in blue. The 12-h positions of Danielle ("d"), Earl ("e"), Fiona ("f"), and Gaston ("g") are shown for the same 48-h period. Time series of mean (b) potential temperature (K) and (c) pressure (hPa) for air parcels released at 0000 UTC 29 Aug from over and northeast of Earl (green) and on the east flank of the upper-level trough (blue). (e),(f) As in (b),(c), but for air parcels released at 0000 UTC 3 Sep over and northeast of Fiona (green) and originating over North America (blue). Error bars in (b),(c),(e),(f) mark ±1.0 standard deviation.

b. *Motion error diagnosis*

The TC motion error diagnostic equation developed by Galarneau and Davis (2013) will be used to examine the large position errors for forecasts of Danielle and Earl in the GEFS control member forecast initialized at 0000 UTC 26 August 2010. To determine the sources of TC motion forecast errors, the

TC steering flow is computed following Galarneau and Davis (2013, see their section 2b) as the area- and vertically averaged environment wind (with the TC removed using vorticity inversion) that best matches the motion of the TC based on positions at ±12 h. The vertical extent of the steering layer ranged from 150 to 650 hPa with a fixed bottom at 850 hPa.[6] The horizontal extent of the steering layer ranged from 1° to 8° from the TC center.

Following the methodology of Galarneau and Davis (2013, see their section 2c), the TC motion error diagnostic equation is defined as

$$\underbrace{\mathbf{V}_m - \mathbf{V}_o}_{\text{motion error}} = \underbrace{\frac{1}{p_b - p_{t,o}} \int_{p_{t,o}}^{p_b} (\hat{\mathbf{v}}_m - \mathbf{v}_o)\, dp}_{\text{environment wind error}} + \underbrace{\frac{1}{p_b - p_{t,m}} \int_{p_{t,m}}^{p_b} -(\hat{\mathbf{v}}_m - \mathbf{v}_m)\, dp}_{\text{radius error}}$$
$$+ \underbrace{\frac{1}{p_b - p_{t,m}} \left[\int_{p_{t,o}}^{p_b} \left(\frac{p_{t,m} - p_{t,o}}{p_b - p_{t,o}} \right) \hat{\mathbf{v}}_m\, dp + \int_{p_{t,m}}^{p_{t,o}} \hat{\mathbf{v}}_m\, dp \right]}_{\text{depth error}} + \text{residual}, \tag{7}$$

where $p_b = 850$ hPa, and p_t is defined as the top of the steering layer. The subscripts "m" and "o" represent the forecast and analysis, respectively. Two area-average environment wind values are computed for the forecasted storm. The first uses the best match radius for the forecasted storm and is defined as $\mathbf{v}_m$. The second uses the best match radius for the observed storm (derived from the CFSR) and is defined as $\hat{\mathbf{v}}_m$. The area-average environment wind value for the observed storm is computed using the best match radius for the observed storm and is defined as $\mathbf{v}_o$. The actual motion of the forecasted and observed storm is defined $\mathbf{V}_m$ and $\mathbf{V}_o$, respectively. The left-hand side of (7) represents the actual motion error of the forecasted TC, while the right-hand side computes the relative contributions of errors in the environment wind, differences in horizontal extent (radius) and depth between the forecasted and observed TC steering flow, and a residual error that arises from differences between the steering layer wind and the actual TC motion and uncertainties in the steering layer radius and depth values.

The westward position errors for Danielle began immediately in the GEFS control member forecast (Fig. 14a). By 1200 UTC 26 August (12-h forecast), Danielle had a larger westward component in its motion in the forecast compared to observations. The definition of the steering layer for the forecasted and observed Danielle was 850–200 hPa and 850–250 hPa, respectively, using a radius of 3° from the center. The motion error diagnostic equation at this time showed that there was a small contribution in motion error from the residual term and arising from a small difference in the steering layer depth (Fig. 15a). Danielle's forecast south-southwestward motion error near 1.2 m s^{-1} comprised primarily a south-southwestward environment wind error near 1.5 m s^{-1} in the 850–250-hPa layer. This environment wind error was driven by a cyclonic circulation error (labeled "C") east and an anticyclonic shear error (labeled "A") north of Danielle (Fig. 15b). These circulation errors were associated with a subtropical anticyclone that was weaker (as measured by anticyclonic vorticity just east of Danielle) and displaced east by about 2° of longitude in the forecast, and a trough in the midlatitude westerlies that was weaker (as measured by cyclonic vorticity northeast of Danielle) in the forecast (Figs. 16a,b). In all, these errors in nearby synoptic-scale circulation systems steered Danielle on a more westward course resulting in the westward position error that rapidly developed by 12 h and increased thereafter with increasing forecast lead (Fig. 14a).

The track forecast for TC Earl was characterized primarily by a slow error through 84 h as it moved westward across the tropical North Atlantic. The forecasted position of Earl began to rapidly depart from the observed system after 84 h, however, as the forecasted TC moved north-northwestward in the subtropics near 55°–60°W while the observed TC continued west-northwestward to just north of Puerto Rico by 0000 UTC 31 August (Fig. 14a). To determine the sources of forecast error that occurred after 84 h, the storm motion error diagnostic was computed for the 84-h forecast verifying at 1200 UTC 29 August. The definition of the steering layer for both the forecasted and observed Earl was 850–300 hPa using a radius of 3° from the center. The motion error diagnostic at this time shows that Earl's forecast east-northeastward motion error over 2 m s^{-1} comprised primarily a northeastward environment wind error near 1.6 m s^{-1} in the 850–300-hPa layer (Fig. 15c). While there

[6] For example, if the vertical extent of the steering layer is 150 hPa, the layer is defined as 850–700 hPa.

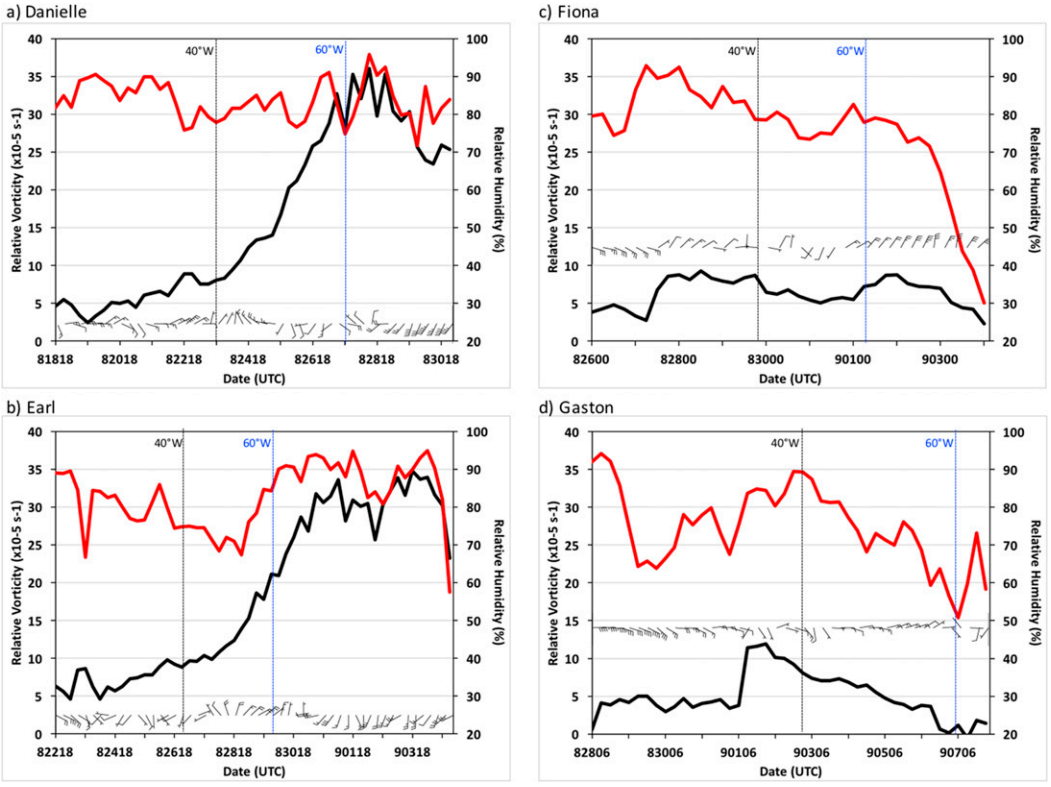

FIG. 10. Time series of 600-hPa relative vorticity (10^{-5} s^{-1}; black line) and 700–500-hPa layer-mean relative humidity (%; red line) averaged within 2° of the storm center, and 900–200-hPa vertical wind shear (half barb = 2.5 m s^{-1}; full barb = 5.0 m s^{-1}) averaged within 3° of the storm center with the TC removed as described in section 2 for (a) Danielle, (b) Earl, (c) Fiona, and (d) Gaston. Times when the TC reached 40° and 60°W are marked by a black dashed line and a blue dashed line, respectively.

are large errors in the environment wind well northwest of Earl associated with errors in the forecast of Danielle's position, the northeastward environment wind error is associated with cyclonic circulation errors just northwest and southwest of Earl (Fig. 15d). The cyclonic circulation error on the northwest side of Earl is related to the model forecast errors associated with Danielle's position and interaction with the midlatitude trough to the west. In the forecast, Danielle was located farther southwest compared to the analysis, which delayed its interaction with the trough to the northwest (Figs. 16c,d). As a result, the ridge axis to the east of Danielle and west of Earl was located farther west than observed (Fig. 16d). In the analysis, Danielle was strongly interacting with and being steered northeastward by the trough to the west (Fig. 16c). Thus, the ridge axis between Danielle and Earl was located farther east and was closer to Earl on its north side. The lack of anticyclonic vorticity just north of Earl (and also southwest of Earl) in the forecast produced a southwesterly steering flow error resulting in Earl's early recurvature in the forecast.

In summary, examination of the forecast positions of Danielle and Earl in the GEFS control member forecast initialized at 0000 UTC 26 August showed that errors in the environment wind field were the primary sources of the large position errors. For Danielle, the environment wind errors were driven by structure and intensity errors of nearby synoptic-scale circulation features in the midlatitudes. For Earl, the environment wind errors were driven by position errors in the forecast of Danielle and the structure of the ridge east of Danielle. Errors in the structure of the ridge were related to errors in Danielle's location, which was modulated by the degree of interaction between Danielle and the upstream midlatitude trough. This one case example nicely highlights the difficult forecast challenge posed by TCs that occur in close proximity in time and space in a rapidly evolving synoptic-scale flow pattern.

7. Conclusions

This paper documented the relevant multiscale processes that influenced the development and life cycle of

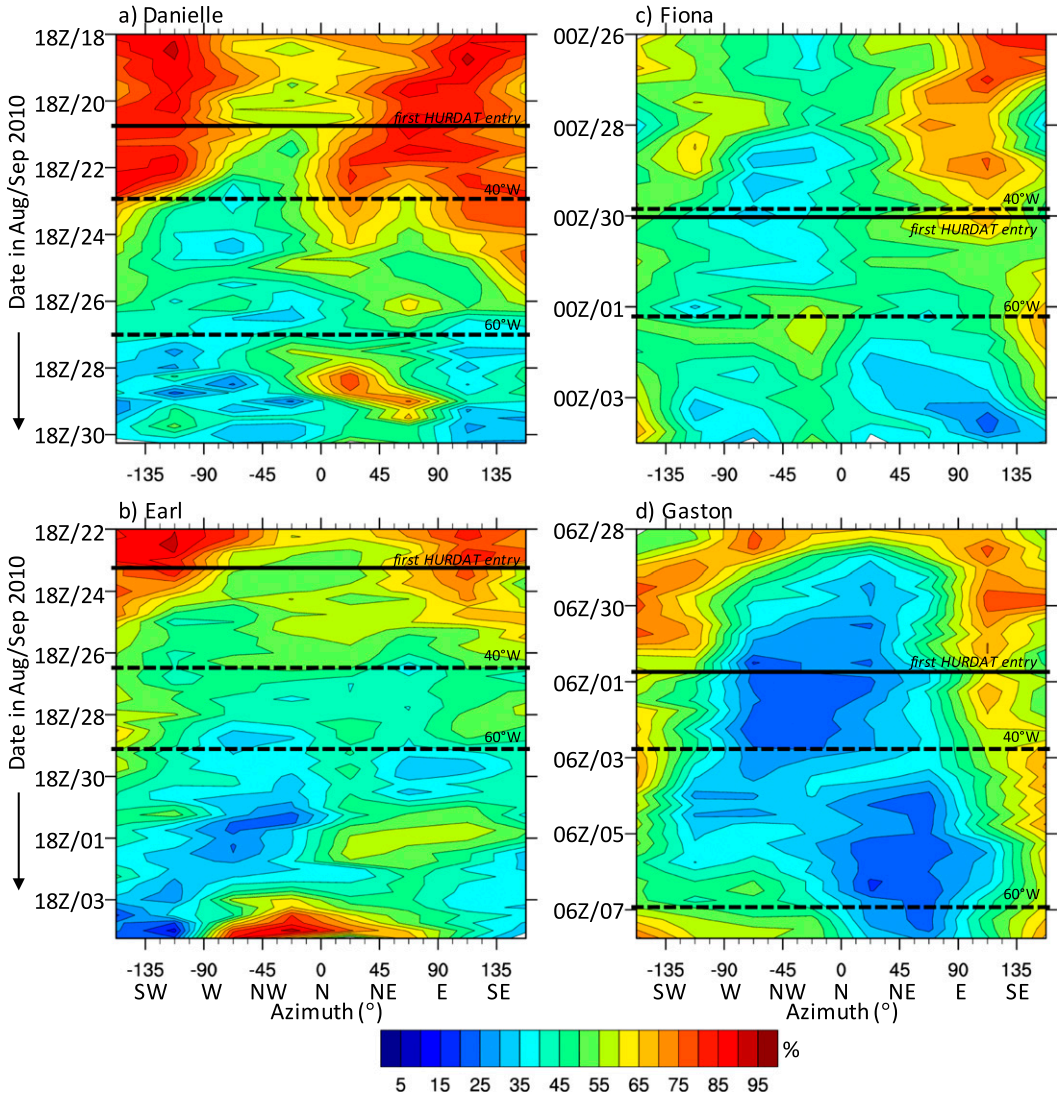

FIG. 11. Time–azimuth diagram of 700–500-hPa layer-mean relative humidity (shaded according to the color bar in %) averaged in the 2°–10° radial band for (a) Danielle, (b) Earl, (c) Fiona, and (d) Gaston. The CFSR data were interpolated to a cylindrical grid prior to averaging. Times when the TC reached 40° and 60°W are marked by a black dashed line. The time of the first entry in the HURDAT is marked by a black solid line.

four TCs in the North Atlantic basin in 2010. These TCs—Danielle, Earl, Fiona, and Gaston—occurred in close proximity in time and space much like the MTCE cases previously described in the literature (e.g., Krouse and Sobel 2010; Schenkel 2016, 2017). The unique aspect of this paper is the analysis and documentation of how four TCs in close proximity interacted with each other and the synoptic-scale flow over the North Atlantic basin, and how this interaction influenced the ability of these TCs to develop. Examination of the forecast skill for the GEFS reforecasts show that the day-5 anomaly correlations were reduced relative to climatology while these four TCs moved over the Atlantic and recurved into midlatitudes. This result highlights the importance in understanding the multiscale processes that influence TC development and movement, and in understanding the linkages between TC evolution and the surrounding environment.

The synoptic-scale flow over the midlatitude North Atlantic was initially zonally oriented prior to the recurvature of TC Danielle on 27 August 2010. A midlatitude RWT that originated over the western North Pacific triggered extratropical cyclogenesis events over extreme eastern North America and the eastern Atlantic. This RWT and attendant cyclogeneses produced downstream impacts, with the synoptic-scale flow pattern becoming more meridional over the North Atlantic.

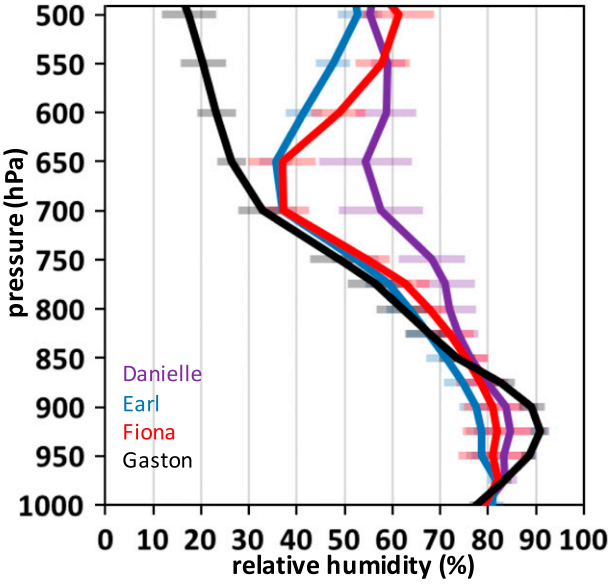

FIG. 12. Vertical profile of area-mean relative humidity in the 22.5°–67.5° azimuth and 2°–10° radial bands time averaged for the 72-h period centered on the time when the TC is located at 50°W for Danielle (purple), Earl (blue), Fiona (red), and Gaston (black). Error bars mark ±1.0 standard deviation.

The recurvature of TC Danielle further enhanced the meridional flow over the North Atlantic. Similar downstream impacts have been documented for recurving TCs over the west Pacific that trigger RWTs (e.g., Torn and Hakim 2015).

The increased meridional flow over the North Atlantic had two foremost consequences. First, it allowed for upper-level troughs to penetrate into the subtropics and provide regions of enhanced vertical wind shear. For instance, the upper-level potential temperature gradient on the west side of the upper-level trough east of TC Danielle was enhanced by potentially warm upper-level outflow associated with Danielle, which helped to strengthen the northerly flow and attendant vertical shear over and northeast of TC Earl. Similar flow interactions occurred as TC Earl recurved and induced large vertical shear over Fiona. This impact of diabatic outflow on upper-level PV gradients and jet intensification was similarly documented by Grams and Archambault (2016) during extratropical transition. Second, the increased meridional flow allowed for dry air to develop in the subtropical central and eastern Atlantic. This dry air inhibited the development of TC Gaston, which was similarly documented by Davis and Ahijevych (2012) using dropsonde observations collected during the Pre-Depression Investigation of Cloud-Systems in the Tropics (Montgomery et al. 2012) field program.

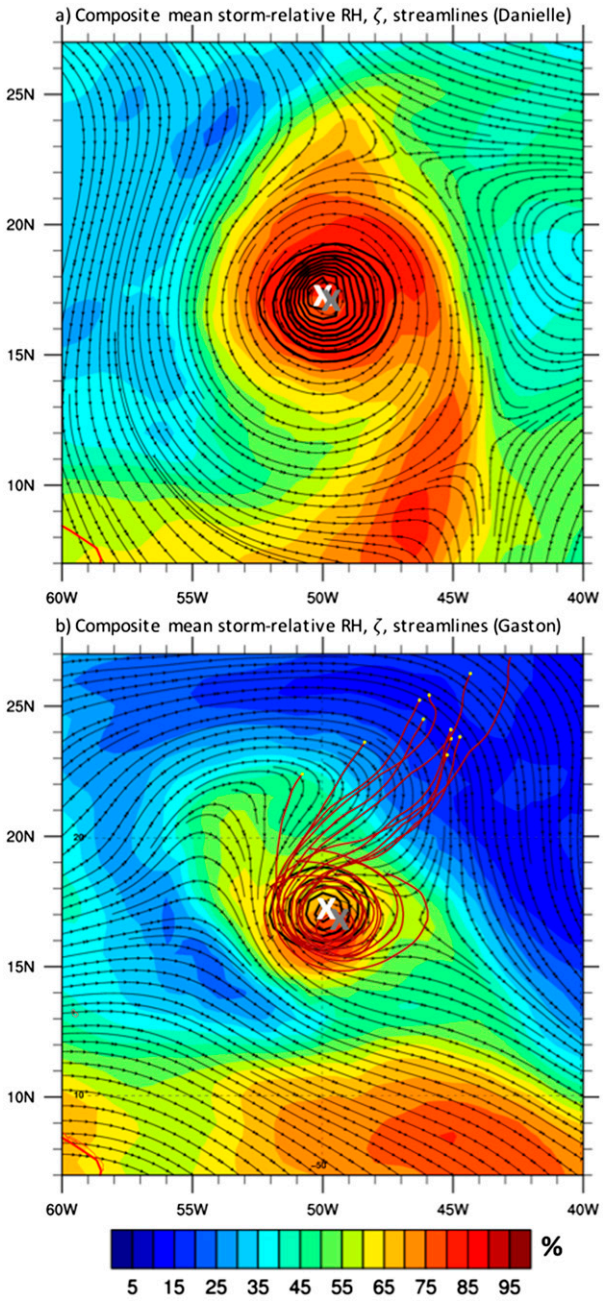

FIG. 13. Composite mean 700–500-hPa layer-mean relative humidity (shaded according to the color bar in %), relative vorticity (solid black contours every 4.0×10^{-5} s^{-1} starting at 4.0×10^{-5} s^{-1}), and storm-relative streamlines (thin black contours with arrow heads) time averaged in storm-relative coordinates for the 72-h period centered on the time in which (a) Danielle and (b) Gaston were located at 50°W. In (b), selected 84-h backward air parcel trajectories (red lines) released in the 700–500-hPa layer from grid points marked × at 1200 UTC 5 Sep 2010 are plotted in storm-relative coordinates. The trajectory end points are marked by a yellow-filled circle.

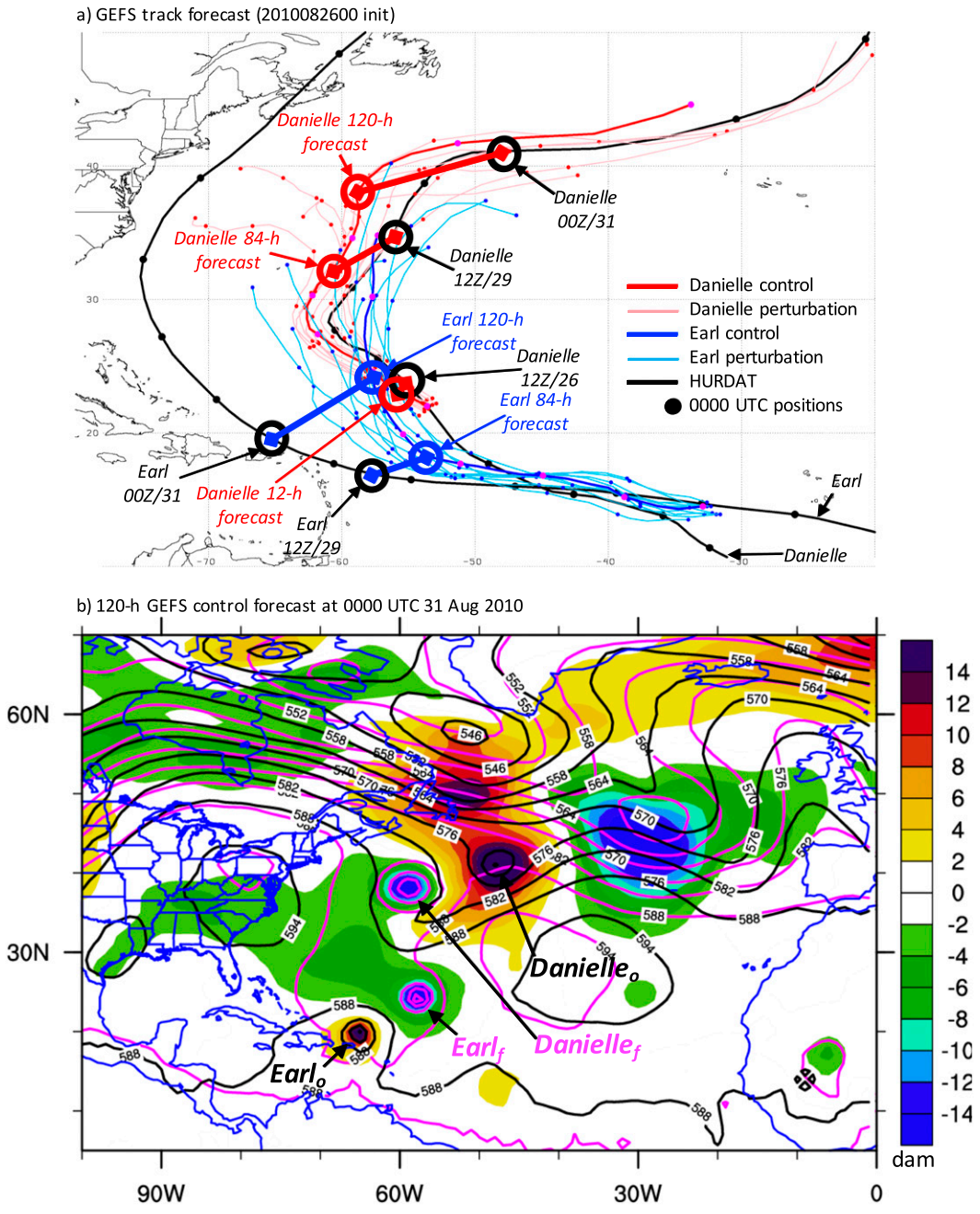

FIG. 14. (a) HURDAT and GEFS track forecasts initialized at 0000 UTC 26 Aug 2010 for Danielle and Earl. The HURDAT tracks are shown in black, while the GEFS control member forecast tracks for Danielle and Earl are shown in red and blue, respectively. The GEFS perturbation member track forecasts for Danielle and Earl are shown in pink and light blue, respectively. TC positions are marked at 0000 UTC by a color-filled circle. Key forecast and corresponding verifying times are marked by open-filled circles. Track errors for Danielle (red) and Earl (blue) at key times are indicated by a thick line segment. (b) GEFS control member 120-h forecast 500-hPa height (magenta contours every 6 dam), 500-hPa height error (forecast minus CFSR; shaded according to the color bar in dam), and verifying CFSR 500-hPa height (black contours every 6 dam) at 0000 UTC 31 Aug 2010. Positions of Danielle and Earl in the forecast and verifying analysis are indicated.

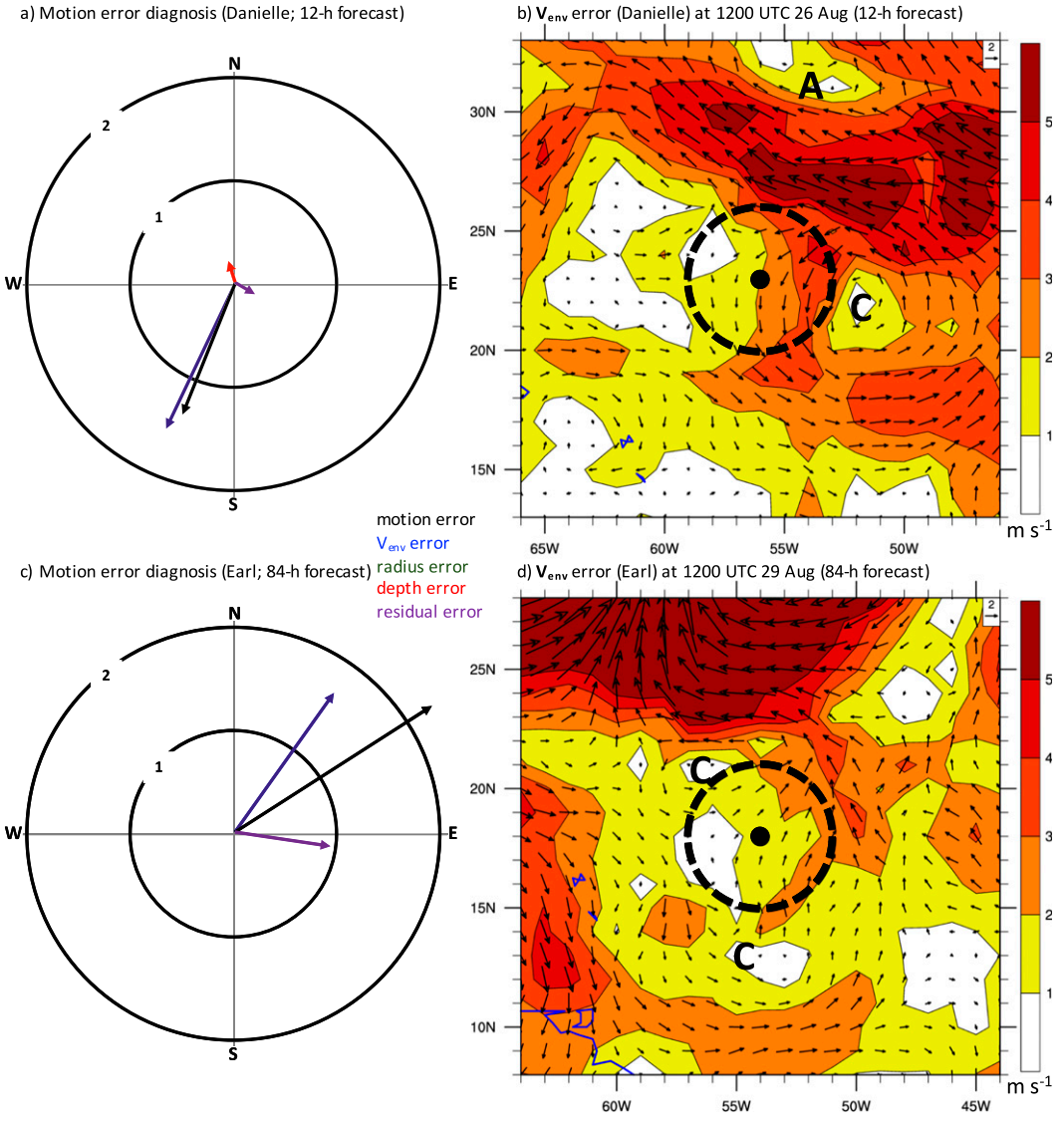

FIG. 15. TC motion error diagnostic equation terms (vector arrows in m s^{-1}) for the GEFS control member (a) 12-h forecast of Danielle verifying at 1200 UTC 26 Aug 2010 and (c) 84-h forecast of Earl verifying at 1200 UTC 29 Aug 2010. The arrows for each term are color coded by the key. An arrow is not plotted if the term = 0. (b) GEFS control member 12-h forecast environment wind error (arrows with magnitude shaded according to the color bar in m s^{-1}) averaged in the 850–250-hPa layer for Danielle. (d) As in (b), but for the 84-h forecast averaged in the 850–300-hPa layer for Earl. The grids were shifted so the observed and forecasted TCs were located at the same position marked by the black-filled circle. The dashed open-filled circle marks the radius (3°) used for the steering layer flow. Selected cyclonic and anticyclonic circulation errors are marked "C" and "A," respectively.

The multiscale processes that connect each of these four TCs over the North Atlantic are complex and present a formidable challenge for operational forecasting. While the prediction of TC track has gained much skill over the last 40 years, prediction of intensity has not (Rappaport et al. 2009). Furthermore, the prediction of TC genesis in the medium range has proven difficult in global numerical weather prediction models (Halperin et al. 2013). Part of the issue, perhaps, is having a numerical weather prediction model that can predict the multiscale physical processes over disparate regions of the hemisphere, rather than just locally over the disturbance of interest. In the case presented here, the ability to predict the structure of synoptic-scale circulation features near the TCs and the interaction between the TCs and the midlatitude trough/RWT are important factors in the ability to accurately predict the track of subsequent TCs.

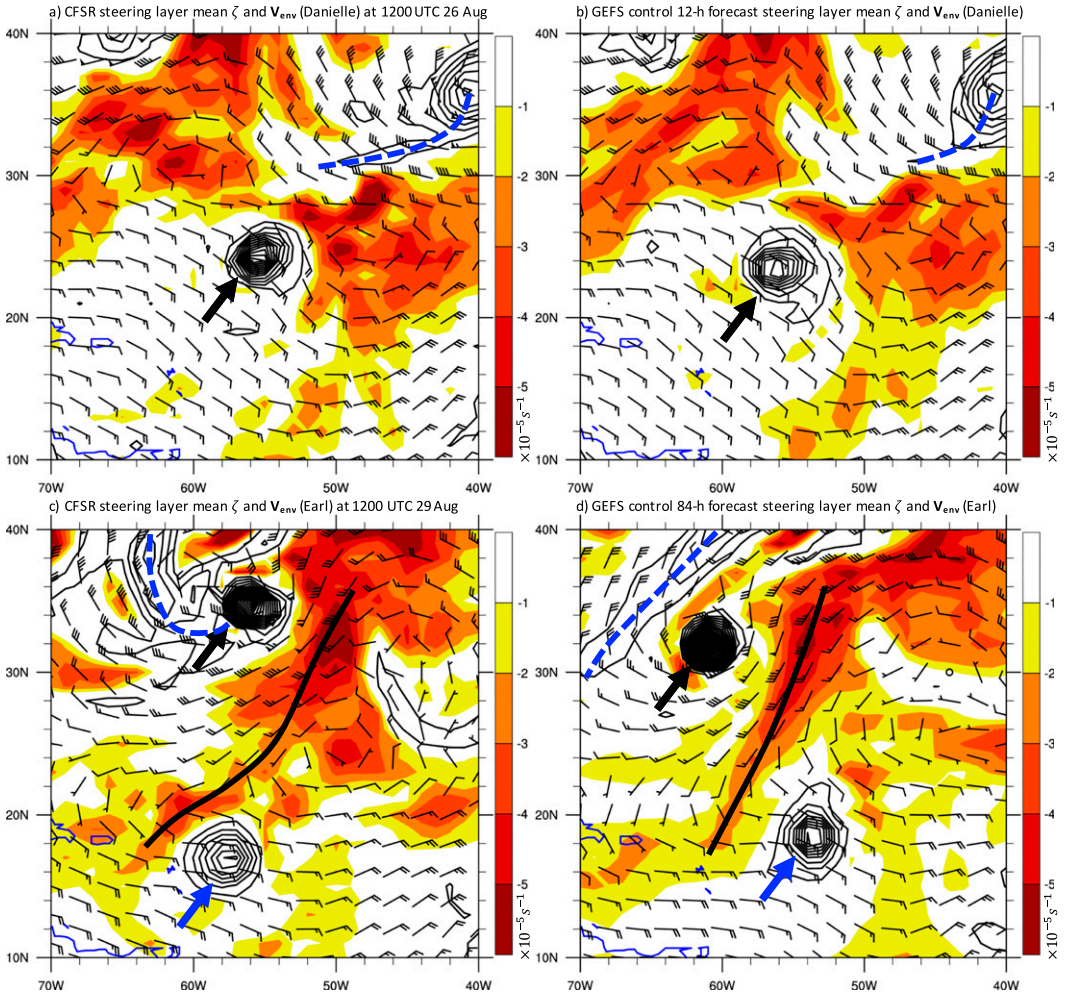

FIG. 16. Steering layer mean relative vorticity (anticyclonic shaded according to the color bar in $\times 10^{-5}\,s^{-1}$; cyclonic plotted in black solid contours every $4.0 \times 10^{-5}\,s^{-1}$ starting at $2.0 \times 10^{-5}\,s^{-1}$), and environment wind (half barb = $2.5\,m\,s^{-1}$; full barb = $5.0\,m\,s^{-1}$; pennant = $25.0\,m\,s^{-1}$) for Danielle in the (a) CFSR and (b) 12-h GEFS control member forecast verifying at 1200 UTC 26 Aug 2010. (c),(d) As in (a),(b), but for Earl in the (c) CFSR and (d) 84-h GEFS control member forecast verifying at 1200 UTC 29 Aug 2010. The steering layer is defined as the 850–250-hPa layer in (a),(b) and 850–300-hPa layer in (c),(d). Danielle and Earl are marked by thick black and blue arrows, respectively. Key midlatitude trough features are marked by a blue dashed line. Key ridge axes are marked by a black solid line.

Future research opportunities for these periods of interacting TCs over the North Atlantic include two possible directions. First, synoptic analysis from a Lagrangian perspective of North Atlantic MTCE cases, such as those identified in the climatology by Schenkel (2016), needs to be conducted. This climatology will allow for identification of the statistically significant behavior and evolution across a series of similar cases. Second, numerical modeling experiments should be conducted to explore the relevant physical and dynamical processes during TC–TC and TC–environment interactions. For instance, ensemble-based sensitivity techniques (e.g., Torn and Hakim 2008) can be used to quantitatively demonstrate the sensitivity of TC development to vertical wind shear and moisture in the subtropics during these periods of interacting TCs. This ensemble sensitivity analysis technique has been successfully used in previous studies to quantitatively examine how vertical wind shear and moisture can impact TC development and track (e.g., Torn et al. 2015).

Acknowledgments. This article arose from the first author's M.S. research at The University of Arizona. The authors thank Chris Castro and Ave Arellano (The University of Arizona) for their valuable feedback on the research presented. Comments from two anonymous

reviewers helped to improve the manuscript. This research was supported by The University of Arizona Office of Research and Discovery (ORD) and Water, Environmental, and Energy Solutions (WEES). Partial support for diagnosis of the GEFS TC track forecasts was originally provided by NOAA HFIP Award NA12NWS4680005.

REFERENCES

Archambault, H. M., L. F. Bosart, D. Keyser, and J. M. Cordeira, 2013: A climatological analysis of the extratropical flow response to recurving western North Pacific tropical cyclones. *Mon. Wea. Rev.*, **141**, 2325–2346, https://doi.org/10.1175/MWR-D-12-00257.1.

——, D. Keyser, L. F. Bosart, C. A. Davis, and J. M. Cordeira, 2015: A composite perspective of the extratropical flow response to recurving western North Pacific tropical cyclones. *Mon. Wea. Rev.*, **143**, 1122–1141, https://doi.org/10.1175/MWR-D-14-00270.1.

Atallah, E. H., and L. F. Bosart, 2003: The extratropical transition and precipitation distribution of Hurricane Floyd (1999). *Mon. Wea. Rev.*, **131**, 1063–1081, https://doi.org/10.1175/1520-0493(2003)131<1063:TETAPD>2.0.CO;2.

Bosart, L. F., and F. Sanders, 1981: The Johnstown flood of July 1977: A long-lived convective system. *J. Atmos. Sci.*, **38**, 1616–1642, https://doi.org/10.1175/1520-0469(1981)038<1616:TJFOJA>2.0.CO;2.

——, B. J. Moore, J. M. Cordeira, and H. M. Archambault, 2017: Interactions of North Pacific tropical, midlatitude, and polar disturbances resulting in linked extreme weather events over North America in October 2007. *Mon. Wea. Rev.*, **145**, 1245–1273, https://doi.org/10.1175/MWR-D-16-0230.1.

Bracken, W. E., and L. F. Bosart, 2000: The role of synoptic-scale flow during tropical cyclogenesis over the North Atlantic Ocean. *Mon. Wea. Rev.*, **128**, 353–376, https://doi.org/10.1175/1520-0493(2000)128<0353:TROSSF>2.0.CO;2.

Brammer, A. B., and C. D. Thorncroft, 2015: Variability and evolution of African easterly wave structures and their relationship with tropical cyclogenesis over the eastern Atlantic. *Mon. Wea. Rev.*, **143**, 4975–4995, https://doi.org/10.1175/MWR-D-15-0106.1.

Davis, C. A., 2015: The formation of moist vortices and tropical cyclones in idealized simulations. *J. Atmos. Sci.*, **72**, 3499–3516, https://doi.org/10.1175/JAS-D-15-0027.1.

——, and L. F. Bosart, 2003: Baroclinically induced tropical cyclogenesis. *Mon. Wea. Rev.*, **131**, 2730–2747, https://doi.org/10.1175/1520-0493(2003)131<2730:BITC>2.0.CO;2.

——, and D. A. Ahijevych, 2012: Mesoscale structural evolution of three tropical weather systems observed during PREDICT. *J. Atmos. Sci.*, **69**, 1284–1305, https://doi.org/10.1175/JAS-D-11-0225.1.

——, and ——, 2013: Thermodynamic environments of deep convection in Atlantic tropical disturbances. *J. Atmos. Sci.*, **70**, 1912–1928, https://doi.org/10.1175/JAS-D-12-0278.1.

——, C. Snyder, and A. C. Didlake, 2008: A vortex-based perspective of eastern Pacific tropical cyclone formation. *Mon. Wea. Rev.*, **136**, 2461–2477, https://doi.org/10.1175/2007MWR2317.1.

Dickinson, M. J., L. F. Bosart, W. E. Bracken, G. J. Hakim, D. M. Schultz, M. A. Bedrick, and K. R. Tyle, 1997: The March 1993 Superstorm cyclogenesis: Incipient phase synoptic- and convective-scale flow interaction and model performance. *Mon. Wea. Rev.*, **125**, 3041–3072, https://doi.org/10.1175/1520-0493(1997)125<3041:TMSCIP>2.0.CO;2.

Dunkerton, T. J., M. T. Montgomery, and Z. Wang, 2009: Tropical cyclogenesis in a tropical wave critical layer: Easterly waves. *Atmos. Chem. Phys.*, **9**, 5587–5646, https://doi.org/10.5194/acp-9-5587-2009.

Galarneau, T. J., Jr., and C. A. Davis, 2013: Diagnosing forecast errors in tropical cyclone motion. *Mon. Wea. Rev.*, **141**, 405–430, https://doi.org/10.1175/MWR-D-12-00071.1.

——, R. McTaggart-Cowan, L. F. Bosart, and C. A. Davis, 2015: Development of North Atlantic tropical disturbances near upper-level potential vorticity streamers. *J. Atmos. Sci.*, **72**, 572–597, https://doi.org/10.1175/JAS-D-14-0106.1.

Gall, R., F. Toepfer, F. Marks, and E. Rappaport, 2014: National Oceanic and Atmospheric Administration Hurricane Forecast Improvement Project years five to ten strategic plan. Tech. Rep. HFIP2014-1.1a, NOAA/Hurricane Forecast Improvement Project, 44 pp., http://www.hfip.org/documents/HFIP_StrategicPlan_Yrs5-10_Nov05_2014_Update.pdf.

Ge, X., T. Li, and M. Peng, 2013: Effects of vertical shears and midlevel dry air on tropical cyclone developments. *J. Atmos. Sci.*, **70**, 3859–3875, https://doi.org/10.1175/JAS-D-13-066.1.

Grams, C. M., and H. M. Archambault, 2016: The key role of diabatic outflow in amplifying the midlatitude flow: A representative case study of weather systems surrounding western North Pacific extratropical transition. *Mon. Wea. Rev.*, **144**, 3847–3869, https://doi.org/10.1175/MWR-D-15-0419.1.

Gray, W. M., 1968: Global view of the origin of tropical disturbances and storms. *Mon. Wea. Rev.*, **96**, 669–700, https://doi.org/10.1175/1520-0493(1968)096<0669:GVOTOO>2.0.CO;2.

Halperin, D. J., H. E. Fuelberg, R. E. Hart, J. H. Cossuth, P. Sura, and R. J. Pasch, 2013: An evaluation of tropical cyclone genesis forecasts from global numerical models. *Wea. Forecasting*, **28**, 1423–1445, https://doi.org/10.1175/WAF-D-13-00008.1.

Hamill, T. M., G. T. Bates, J. S. Whitaker, D. R. Murray, M. Fiorino, T. J. Galarneau, Y. Zhu, and W. Lapenta, 2013: NOAA's second-generation global medium-range ensemble reforecast dataset. *Bull. Amer. Meteor. Soc.*, **94**, 1553–1565, https://doi.org/10.1175/BAMS-D-12-00014.1.

Hopsch, S. B., C. D. Thorncroft, and K. R. Tyle, 2010: Analysis of African easterly wave structures and their role in influencing tropical cyclogenesis. *Mon. Wea. Rev.*, **138**, 1399–1419, https://doi.org/10.1175/2009MWR2760.1.

Kiladis, G. N., C. D. Thorncroft, and N. M. J. Hall, 2006: Three-dimensional structure and dynamics of African easterly waves. Part I: Observations. *J. Atmos. Sci.*, **63**, 2212–2230, https://doi.org/10.1175/JAS3741.1.

Komaromi, W. A., 2013: An investigation of composite dropsonde profiles for developing and nondeveloping tropical waves during the 2010 PREDICT field campaign. *J. Atmos. Sci.*, **70**, 542–558, https://doi.org/10.1175/JAS-D-12-052.1.

Krouse, K. D., and A. H. Sobel, 2010: An observational study of multiple tropical cyclone events in the western North Pacific. *Tellus*, **62A**, 256–265, https://doi.org/10.1111/j.1600-0870.2010.00435.x.

Landsea, C., and Coauthors, 2004: The Atlantic Hurricane Database reanalysis project: Documentation for the 1851–1910 alterations and additions to the HURDAT database. *Hurricanes and Typhoons: Past, Present, and Future,* R. J. Murname and K.-B. Liu, Eds., Columbia University Press, 177–221.

Massacand, A. C., H. Wernli, and H. C. Davies, 1998: Heavy precipitation on the alpine southside: An upper-level precursor. *Geophys. Res. Lett.*, **25**, 1435–1438, https://doi.org/10.1029/98GL50869.

McBride, J. L., and R. Zehr, 1981: Observational analysis of tropical cyclone formation. Part II: Comparison of non-developing versus developing systems. *J. Atmos. Sci.*, **38**, 1132–1151, https://doi.org/10.1175/1520-0469(1981)038<1132:OAOTCF>2.0.CO;2.

Montgomery, M. T., and Coauthors, 2012: The Pre-Depression Investigation of Cloud-Systems in the Tropics (PREDICT) Experiment: Scientific basis, new analysis tools, and some first results. *Bull. Amer. Meteor. Soc.*, **93**, 153–172, https://doi.org/10.1175/BAMS-D-11-00046.1.

Nolan, D. S., 2007: What is the trigger for tropical cyclogenesis? *Aust. Meteor. Mag.*, **56**, 241–266.

Orlanski, I., 1975: A rational subdivision of scales for atmospheric processes. *Bull. Amer. Meteor. Soc.*, **56**, 527–530.

——, and J. P. Sheldon, 1995: Stages in the energetics of baroclinic systems. *Tellus*, **47A**, 605–628, https://doi.org/10.3402/tellusa.v47i5.11553.

Rappaport, E. N., and Coauthors, 2009: Advances and challenges at the National Hurricane Center. *Wea. Forecasting*, **24**, 395–419, https://doi.org/10.1175/2008WAF2222128.1.

Rappin, E. D., and D. S. Nolan, 2012: The effect of vertical shear orientation on tropical cyclogenesis. *Quart. J. Roy. Meteor. Soc.*, **138**, 1035–1054, https://doi.org/10.1002/qj.977.

Reed, R. J., D. C. Norquist, and E. E. Recker, 1977: The structure and properties of African wave disturbances as observed during Phase III of GATE. *Mon. Wea. Rev.*, **105**, 317–333, https://doi.org/10.1175/1520-0493(1977)105<0317:TSAPOA>2.0.CO;2.

Riemer, M., and S. C. Jones, 2010: The downstream impact of tropical cyclones on a developing baroclinic wave in idealized scenarios of extratropical transition. *Quart. J. Roy. Meteor. Soc.*, **136**, 617–637, doi:10.1002/qj.605.

Saha, S., and Coauthors, 2010: The NCEP Climate Forecast System Reanalysis. *Bull. Amer. Meteor. Soc.*, **91**, 1015–1057, https://doi.org/10.1175/2010BAMS3001.1.

Schenkel, B. A., 2016: A climatology of multiple tropical cyclone events. *J. Climate*, **29**, 4861–4883, https://doi.org/10.1175/JCLI-D-15-0048.1.

——, 2017: Are multiple tropical cyclone events similar among basins? *J. Climate*, **30**, 5805–5813, https://doi.org/10.1175/JCLI-D-17-0088.1.

Simpson, R. H., and H. Saffir, 1974: The hurricane disaster–potential scale. *Weatherwise*, **27**, 169–186, https://doi.org/10.1080/00431672.1974.9931702.

Smith, R. K., and M. T. Montgomery, 2012: Observations of the convective environment in developing and non-developing tropical disturbances. *Quart. J. Roy. Meteor. Soc.*, **138**, 1721–1739, https://doi.org/10.1002/qj.1910.

Stein, A. F., R. R. Draxler, G. D. Rolph, B. J. B. Stunder, M. D. Cohen, and F. Ngan, 2015: NOAA's HYSPLIT atmospheric transport and dispersion modeling system. *Bull. Amer. Meteor. Soc.*, **96**, 2059–2077, https://doi.org/10.1175/BAMS-D-14-00110.1.

Tao, D., and F. Zhang, 2014: Effect of environmental shear, sea-surface temperature, and ambient moisture on the formation and predictability of tropical cyclones: An ensemble-mean perspective. *J. Adv. Model. Earth Syst.*, **6**, 384–404, https://doi.org/10.1002/2014MS000314.

Thorncroft, C. D., B. J. Hoskins, and M. E. McIntyre, 1993: Two paradigms of baroclinic-wave life-cycle behaviour. *Quart. J. Roy. Meteor. Soc.*, **119**, 17–55, https://doi.org/10.1002/qj.49711950903.

Torn, R. D., and G. J. Hakim, 2008: Ensemble-based sensitivity analysis. *Mon. Wea. Rev.*, **136**, 663–677, https://doi.org/10.1175/2007MWR2132.1.

——, and ——, 2015: Comparison of wave packets associated with extratropical transition and winter cyclones. *Mon. Wea. Rev.*, **143**, 1782–1803, https://doi.org/10.1175/MWR-D-14-00006.1.

——, J. S. Whitaker, P. Pegion, T. M. Hamill, and G. J. Hakim, 2015: Diagnosis of the source of GFS medium-range track errors in Hurricane Sandy (2012). *Mon. Wea. Rev.*, **143**, 132–152, https://doi.org/10.1175/MWR-D-14-00086.1.

Tory, K. J., and W. M. Frank, 2010: Tropical cyclone formation. *Global Perspectives of Tropical Cyclones: From Science to Mitigation*, J. Chan and J. D. Kepert, Eds., World Scientific, 55–91.

Wang, Z., 2012: Thermodynamic aspects of tropical cyclone formation. *J. Atmos. Sci.*, **69**, 2433–2451, https://doi.org/10.1175/JAS-D-11-0298.1.

Zawislak, J., and E. J. Zipser, 2014: A multisatellite investigation of the convective properties of developing and nondeveloping tropical disturbances. *Mon. Wea. Rev.*, **142**, 4624–4645, https://doi.org/10.1175/MWR-D-14-00028.1.